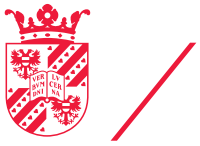

university of groningen / faculty of science and engineering

University of Groningen, Groningen
Bachelor Research Project, Applied Physics

Electrostatic Hexapole & Quadrupole for Guiding Slow BaF Molecules

Author:
Thijs Niemeijer (s3188825)

Examiners:
Steven Hoekstra
Maria Antonietta Loi

July 12, 2020

Abstract

In the Bachelor thesis electrostatic hexapoles and quadrupoles are investigated by simulations done in Python. These hexapoles or/and quadrupoles had the goal to increase the number of accepted molecules in a Stark decelerator. This Stark decelerator is part of a bigger project. In this project the electron electric dipole moment will be measured for Barium Mono-Fluoride molecules. These simulations were done for all the practical problems the project has between the cryogenic source and the Stark decelerator. These problems mostly come from the transversal and longitudinal velocities of the molecules leaving the source.
The highest achieved acceptance for this research is found when there are two guides placed. The front guide has to be a 125 mm hexapole of 4 mm inner radius at applied voltage of 6.5 kV. And the rear guide has to be a 50 cm hexapole of 4 mm inner radius at applied voltage of 6.9 kV. In Figure 29 this situation is displayed.
For future research, this same simulation code is accessible for the NL-eEDM team. These simulations for now only looked at the $|N, m_N\rangle = |10\rangle$ state. But the $|N, m_N\rangle = |20\rangle$ is also especially important for the project.

Contents

1 Introduction

1.1 Historic Overview

"But surely you don't believe that the (spatial) orientation of atoms is something physically real; that is (only) a timetable for the electrons"[1]. Walther Gerlach encountered doubtful colleagues, including Peter Debye, who said this about their experiment prior to its publication. The experimental demonstration, by Otto Stern and Walther Gerlach, on the spatial quantization really succeeded in changing the mind of atomic physicists [2] whom beforehand had regarded the attempt of observing space quantization as a foolish and naive research. The experiment is done by measuring the deflection of a beam of atoms with its magnetic moment when it moves through an inhomogeneous magnetic field, also known as the Zeeman effect. This famous experiment was finished within one year in February of 1922 [3]. No other experiment is more often cited, just for its elegant conceptual simplicity. The first demonstration of the electrical deflection of a beam of polar molecules was shown several years later by a graduate student of Stern, named Erwin Wrede. These essential properties of atoms and molecules were shown almost 100 years ago. Still their relevance is of a high significance. And paved the way for modern-day Atomic physics.

Modern-day atomic physics is busy with finding the proof for proposed laws and stated theories. Such a recent and prominent discovery is that of the Higgs Boson at CERN's Large Hadron Collider (LHC)[4]. These discoveries around and on the Higgs Boson are done to research the charge conjugation (C) and parity (P) violation of the Standard Model (SM). Which could explain the matter-antimatter asymmetry in the Universe. As far for particle physics, the SM is currently the best theory. However, the theory is not complete yet as one thing is still missing in the theory. Which quite essentially, gravity is not included in. And as mentioned earlier, the large surplus of matter versus anti-matter is not predicted by the SM. But recently an interesting paper has been published about this [5]. Doing research on these subjects will improve our understanding of the Universe and life itself.

The experiment that this thesis is written for, is such a research subject. And it concerns the electric dipole moment of an electron (eEDM). If the effective eEDM is nonzero then this will imply that the electron effectively has an a-spherical charge distribution on its spin axis [6]. This is of importance because of the charge conjugation, parity, and time-reversal (CPT). It is shown that the CP-conservation does not hold, thus T-symmetry has to be broken to conserve CPT. As T-conservation does not allow this a-spherical charge distribution within fundamental particles like an electron. And therefore, a non-zero eEDM violates T-symmetry.

For this experiment barium monofluoride (BaF) molecules are decelerated and made into an intense cold beam. And the molecules are then measured for its magnitude of the permanent eEDM with the lowest sensitivity possible. The team predicts to find a sensitivity to an eEDM value of $d_e = 5 \times (10^{-30})\ e \cdot cm$. The schematics of the setup can be seen in Figure 1.

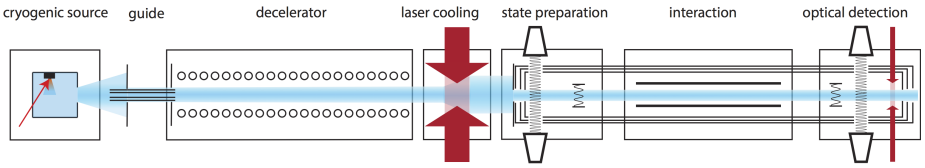

Figure 1: *A schematic overview of the research currently done on the eEDM. A molecule beam is made intense and cold when it is traveling from the left to the right. This image is taken from the original source [7].*

1.2 The NL-eEDM Experiment

To measure the eEDM, BaF molecules are made into a molecular beam source using cryogenic buffer gas methods to cool it down, also see [8][9][10]. This Beam is made cold and slow, so its eEDM is measured more precisely. It can be measured more precisely because of its longer measuring time. The longer measuring time of the molecules decreases the sensitivity. For more on this see the original source [7]. A lot of the BaF molecules are lost due to the transversal expansion and velocities of the beam. As the simplified depiction shows, on the left in Figure 2. The acceptance of the decelerator has, therefore, a loss factor of roughly 29. In order to decrease this, an electrostatic guide(s) is made between the cryogenic source to the Stark decelerator. And this electrostatic guide is the subject of this paper. This guide can be the solution to the large's loss factor problem. As the simplified depiction shows, in the middle and right of Figure 2. The electrostatic guide also solves most of the alignment issues and decreases the loss factor of the source decelerator connection. And with this the sensitivity to an eEDM value can be decreased.

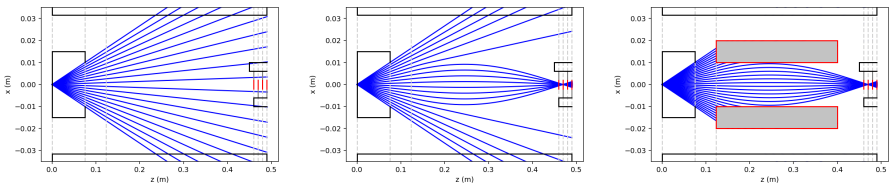

Figure 2: *Hypothetical situations to illustrate our problem and our solution to this problem. On the left you see the cryogenic source and the produced molecules leaving it. The Stark decelerator is depicted with its rings red. In the Middle picture, an electrostatic guide is added. On the right it shows that the remaining molecules will collide with the electrodes of the guide.*

A beam of neutral molecules can be controlled and steered in its motion with an inhomogeneous magnetic or an electric field [11]. Also, both these electrical and magnetic field geometries can be designed in a static field manner to be used to focus or deflect the beam. Furthermore, if the field is time-varying it

can use to decelerate or accelerate molecular beams. This is done in the Stark decelerator of the experiment mentioned above. In figure 3 it is shown how the decelerator looks in the lab. The Stark decelerator will exploit the Stark effect in order to decelerate the molecules. It works as follows; a high voltage is applied to an array of electrodes shaped like rings, through which the molecules travel. In this array a sequence is made of moving regions at low electric field strengths. The molecules that are said to be, low-field seeking, tend to want to stay naturally in the low-field region. Low-field seeking molecules are treated in section 2.3 if more explanation is needed. If then the velocity of these low-field regions is decreased, the molecules will also decrease in velocity. With the simulations of the guide, the goal is to determine the best configuration in geometry and charge that gives the minimal loss factor of molecules reaching the decelerator's low-field regions.

An electrostatic hexapole guide and an electrostatic quadrupole are used, which is an arrangement of six cylindrical electrodes with alternating negative and positive voltages or an arrangement of four cylindrical electrodes with alternating negative and positive voltages, respectively. These electrostatic guides were used for other experiments by the Vrije Universiteit Amsterdam. These guides will be modified and simulated for this particular experiment. Also, some other designs are tested that could be created with a few adjustments done to the already constructed guides.

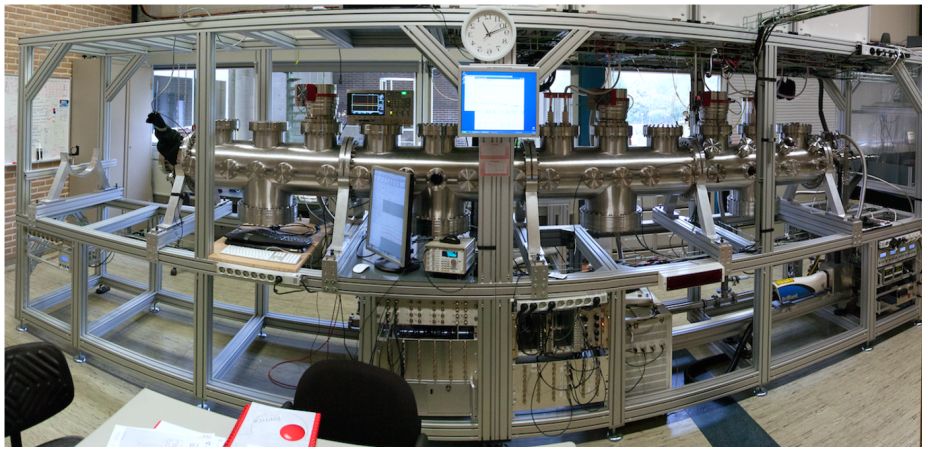

Figure 3: *A side view of the Stark decelerator made by the Van Swinderen Institute and now its modified to fit in the eEDM experiment. The VSI built this 4.5-meter-long decelerator for studying the fundamental symmetry violations of heavy diatomic molecules like BaF with slow beams. This image is taken from the original source [7].*

2 Theory

2.1 Multipole Expansion of the Electric Field in Two Dimensions

J.C. Maxwell himself believed that the electric and magnetic fields would be strains and stresses in an invisible primordial jellylike *Ether*. Later this notion was abandoned due to Special relativity. Maxwell's incorrect assumption shows that the understanding of electric and magnetic fields is not straight forward, even for famous physicists. Often denoted by **E**, it is the function of position in space giving the field direction and magnitude, for further knowledge of the basic principles follow the book referenced [12]. In this section, we will analyze the expansion of the electric field for our electrostatic hexapole & electrostatic quadrupole. For the inhomogeneous electric field inside the hexapole the electric potential Φ obeys the Laplace equation $\nabla^2\mathbf{\Phi} = 0$, if free charges are in absence. The general solution of the Laplace equation in two dimensions, can be expressed as the multipole expansion in cylindrical coordinates:

$$\Phi(r,\theta) = \Phi_0 \left[\sum_{n=1}^{\infty} \frac{a_n}{n} \left(\frac{r}{r_0}\right)^n cos(n\theta) + \sum_{n=1}^{\infty} \frac{b_n}{n} \left(\frac{r}{r_0}\right)^n sin(n\theta) \right] \tag{1}$$

Formula derived from [11][13]. Because we are in cylindrical coordinates $r = (x^2+y^2)^{\frac{1}{2}}$ and $\theta = tan(\frac{y}{x})^{-1}$. (a_n, b_n) are dimensionless constants of the 2n-pole strengths. Respectively, Φ_0 and r_0 are the scaling parameters that characterizes the size of the electrode applied voltages and structure. If we set n = 1 then it will represent a homogeneous electric field. For n = 2 and for n = 3 terms it will represent a quadrupole and hexapole fields, respectively.

The quadrupole or the hexapole field distribution in the transverse plane allows for the low field seeking molecules to be confined and even focused on this plane. This will lead to transverse phase-space *matching* between the Stark decelerator and the source as explained in section 2.4.2. For the quadrupole we know that the electric field at the center should have a magnitude of zero and that it should linearly increase proportional to r from the center. This field can be created for a quadrupole by setting all coefficients of equation 1 to be zero except a_2:

$$\begin{aligned} \Phi(r,\theta) &= \Phi_0 \left[\frac{a_2}{2} \left(\frac{r}{r_0}\right)^2 cos(2\theta) + \frac{b_2}{2} \left(\frac{r}{r_0}\right)^2 sin(2\theta) \right] \\ \Phi(r,\theta) &= \Phi_0 \frac{a_2}{2} \left(\frac{r}{r_0}\right)^2 cos(2\theta) \Leftrightarrow \Phi(x,y) = \Phi_0 \left(a_2 \frac{x^2-y^2}{2r_0^2} \right) \end{aligned} \tag{2}$$

And from $E = -\nabla\Phi$ hence,

$$E(r,\theta) = \Phi_0 r \left[\frac{a_2}{r_0^2} \right] \tag{3}$$

For the hexapoles, we know that the electric field at the center should have a magnitude of zero and that the it should quadratically increase proportional to r from the center. This field can be created for a hexapole by setting all coefficients of equation 1 to be zero except a_3:

$$\begin{aligned} \Phi(r,\theta) &= \Phi_0 \left[\frac{a_3}{3} \left(\frac{r}{r_0} \right)^3 cos(3\theta) + \frac{b_3}{3} \left(\frac{r}{r_0} \right)^3 sin(3\theta) \right] \\ \Phi(r,\theta) = \Phi_0 \frac{a_3}{3} \left(\frac{r}{r_0} \right)^3 cos(3\theta) &\Leftrightarrow \Phi(x,y) = \Phi_0 \left(a_3 \frac{x^3 - 3xy^2}{3r_0^3} \right) \end{aligned} \tag{4}$$

And from $E = -\nabla\Phi$ hence,

$$E(r,\theta) = \Phi_0 r^2 \left[\frac{a_3}{r_0^3} \right] \tag{5}$$

From $\vec{F} = -\vec{\nabla} W(E) = \mu_{eff} \vec{\nabla} E$, the Stark shift can be obtained and thus the force on the molecules, which is used in section 2.3.

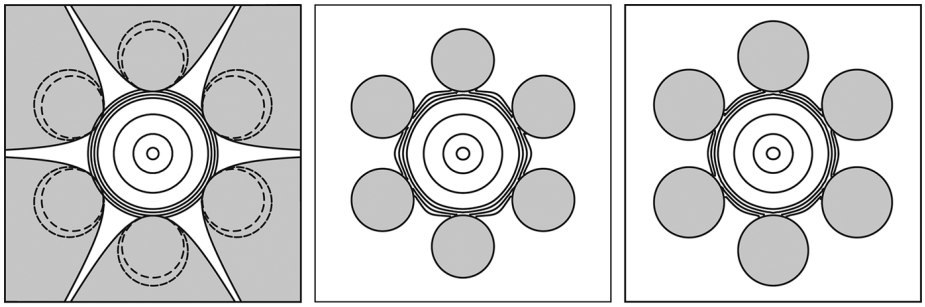

(a) Ideal hexapole (b) Rod radius: *R/2* (c) Rod radius: *0.565R*

Figure 4: *The inner radius R is 3 mm in all geometries. And the potential on the electrodes is ±10 kV. The lines are of the equal electric field strengths. And their values are from the inside out: 1, 10, 40, 80, 90, 100, and 110 kV/cm. (a) The most ideal hexapole with hyperbolic electrodes. (b) Hexapole with the radius of the rods being equal to R/2. (c) Hexapole with the radius of the rods being equal to 0.565R. The outline of the rods is also shown. This image is taken from the original source [11].*

If we were to design the ideal hexapole, the surfaces of the electrodes would have to have the shape of a hyperbole. This surface will then generate the most perfect symmetric electric field distributions within the guide. Unfortunately, the hyperbolic surfaces of the electrodes would come so close to each other, at large radii, that the electrodes will discharge between another. This is prevented by constructing, easier to make, cylindrical electrodes. How this geometry of the cylindrical electrodes corresponds to the hyperbolic surfaces and its produced electric field distribution is shown in Figure 4. From the picture it can be seen

that the most important piece of surface coincides with the ideal hexapole design. So, it can be assumed that this guide will create just as good of an electric field distribution, as the hyperbolic surfaces would. The better approximation of the ideal hexapole field was recommended by Anderson [14] and shows that the rod radius must be of $0.565r_0$ as in Figure 4c.

2.2 Electronic and Vibrational Energy Levels

For the understanding of where the energy splitting comes from, the ground state and the excited state is highlighted here. Most work is based on previously done work by a colleague. If we look at molecules the smallest energy splitting is the one between rotational levels, these are usually in the range of $0.1 - 10$ cm^{-1}. After that the vibrational levels have a larger splitting and these usually have this in the range of $10^2 - 10^4$ cm^{-1} and the largest energy splitting is between the electronic states and these are usually in the range of $10^4 - 10^5$ cm^{-1}. We will now look at some of the energy level structure of electronic states. The electronic states are in this notation denoted by S, which is the spin, Λ and Ω denote the projection of the orbital angular momentum and the total angular momentum respectively along the internuclear axis. And the +/- sign denotes the refection symmetry in the electronic state: ${}^{2S+1}\Lambda_{\Omega}^{(+/-)}$.

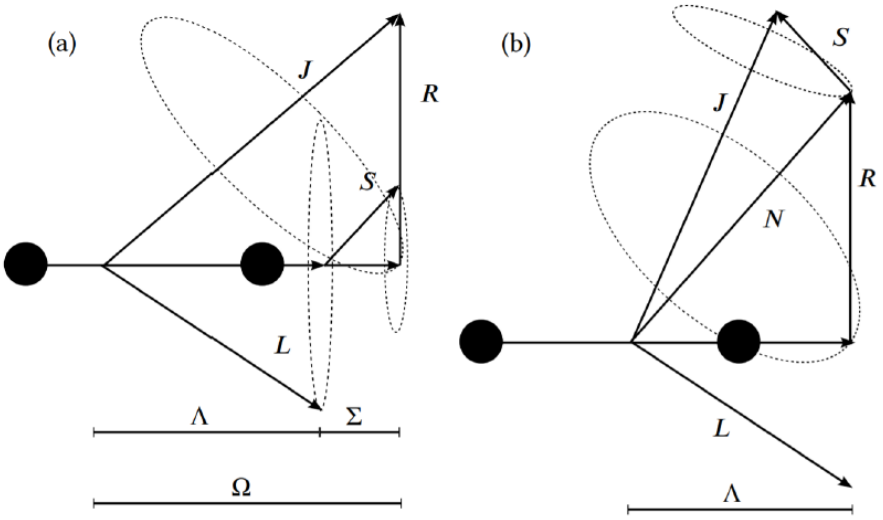

Figure 5: *Clear depiction of the so called Hund's case, with (a) on the left and (b) on the right. This image is taken from the original source [15].*

2.2.1 The $X^2\Sigma^+_{1/2}$ Ground State

This ground state follows the description of Hund's case (b), in this the electronic orbital angular momentum **L** precesses around the internuclear axis [15]. With this the component along the axis is Λ. Therefore, the angular momentum of the nuclei is coupled (**Λ** and **R**). And these form the total electronic angular momentum minus electronic spin **N**. Therefore $\mathbf{N} = \mathbf{R}$ and $\lambda = 0$ for this state. This results in the coupling of **N** with the electronic spin **S** which will give the total electronic angular momentum **J** and with this **J** it will couple with the nuclear spin **I** to form the total angular momentum **F**.

If we now look at the rotational levels of the ground state, then we can describe the energy levels N with the Hamiltonian. Let us look at the $X^2\Sigma_{1/2}$ ground state, the splitting of the rational levels N into J levels which is done by the spin rotation interaction. This all is described by a Hamiltonian [15]:

$$H_{sr} = \gamma\ \mathbf{N}\cdot\mathbf{S} + \frac{1}{2}\gamma_D\{\mathbf{N}\cdot\mathbf{S}, \mathbf{N^2}\} + \frac{1}{2}\gamma_H\{\mathbf{N}\cdot\mathbf{S}, \mathbf{N^4}\} \tag{6}$$

In this Hamiltonian γ gives the electron spin rotation coupling constant [16], γ_D and γ_H are respectively, the quartic and the sextic centrifugal distortion corrections [17]. Remember that **S** give the spin of the valence electrons and that is in our ground state equal to $\frac{1}{2}$. The brackets denoted above indicate that they are anticommutators.

The rotational Hammiltonian is given for the energy in the rotational levels of N:

$$H_{rot} = B\mathbf{N}^2 - D\mathbf{N}^4 + H\mathbf{N}^6 \tag{7}$$

Here N is only the rotational angular momentum thus, here the nuclear spin and the electronic spin are excluded. B, D and H are the rotational constant, the quartic and the sextic centrifugal distortion [16].

And as last, the hyperfine structure of the ground state splits the J level into F levels by coupling **I** (nuclear spin) with **J**: $\mathbf{F} = \mathbf{J} + \mathbf{I}$. The Barium nucleus possesses no nuclear spin, but the Fluorine nucleus has equal to $\frac{1}{2}$. This gives that the J levels will split in hyperfine levels$\rightarrow$ $\mathbf{F} = \mathbf{J} \pm \frac{1}{2}$. Again, the splitting can be described by a Hamiltonian [18]:

$$H_{hfs} = b\ \mathbf{I}\cdot\mathbf{S} + c\ \mathbf{I_z}\cdot\mathbf{S_z} \tag{8}$$

where I_z and S_z are the z-components of I and S. The hfs constant b is the nuclear spin-electron coupling and c here is the nuclear spin-electron spin dipole-dipole interaction. In this ground state, the hyperfine constants for Fluorine are c[F] = 8.224(58) MHz and b[F] 63.509(32) MHz [18].

2.2.2 The $A^2\Pi$ Excited State

This $A^2\Pi$ excited state obeys Hund's case (a) the most. For this case **L** is coupled electrostatically to the internuclear axis. **L** and **S** are spin-orbit interaction couples and Λ and Σ here are the components along the internuclear axis. Ωis

coupled to the angular momentum of the rotating nuclei **R** and forms the total angular momentum **J**. Where Ω is the sum of Λ and Σ, With this Ω is the vector of length of Ω that points along the internuclear axis.

Lets now look at the largest energy splitting in this state which is also known as the Ω-doubling. Furthermore, the splitting is larger than splitting between the vibrational levels. For you to understand you can think of it as similar to the fine structure splitting in atoms. And you can therefore describe this state as two different Ω but with both holding their vibrational levels. From this we can conclude that there are four possible combinations with $|\Pi| = 1$ and $S = \frac{1}{2}$. $\left[\Lambda = \pm 1, \Sigma = \pm\frac{1}{2}\right] \Rightarrow \Omega = |\Lambda \pm \Sigma| = \frac{1}{2}, \frac{3}{2}$. Thus the $A^2\Pi$ state will split into $A^2\Pi_{\frac{1}{2}}$ and $A^2\Pi_{\frac{3}{2}}$. Again, a Hamiltonian can be described to give the energy splitting from these states [15]:

$$H_{so} = A\ \mathbf{L}\cdot\mathbf{S} + \frac{A_{cd}}{2}\left\{\mathbf{N^2}, \mathbf{L}\cdot\mathbf{S}\right\} \tag{9}$$

Here A and A_{cd} are respectively, the spin-orbit coupling constant and the centrifugal distortion [16]. More information about Electronic & Vibrational energy levels is not needed for our calculations. This is because the simulations done use the data gathered earlier by a colleague. For how this data is gathered precisely, please read the original source [19].

2.3 Stark Effect

The Stark effect is the shifting of the spectral lines of molecules and atoms due to an external electric field. The Stark shifted energy levels can be found by calculating the eigenvalues of the Stark Hamiltonian $H_{Stark} = -\vec{\mu}\cdot\vec{E}$. With this the Hamiltonian that calculates the energy of the hyperfine levels if in presence of an electric field is:

$$H = H_{hfs} + H_{Stark} \tag{10}$$

here the H_{hfs} is the previously stated Hamiltonian for the hyperfine structure in equation 8. With the EDM of BaF: $\mu_e = 3.170(3)D$.

Because the molecules come from a cryogenic source, they are cold and are in their ground states. This is also what we want to have for the decelerator and the laser cooling. The stark shift of the lowest three rotational levels of BaF in the electronic ground state is found, with its relation to the applied electric field strength as can be seen in Figure 6. The reason for why higher N levels are preferable for Stark deceleration's is clearly visible. Because of the larger stark shift like in the $|N, |m_N|\rangle = |2, 0\rangle$ state.

The resulting force $\vec{F} = -\vec{\nabla}W(\varepsilon) = \mu_{eff}\vec{\nabla}E$ is oriented in the opposite direction of the electric field gradient. Molecules with positive Stark shift in these states are better known as low field seeking (LFS) as they are repulsed by the field. Molecules with negative Stark shift in these states are better known as high field seeking (HFS) as they are attracted by the field. Molecules that are in the low field seeking states can be focused using hexapolar and/or quadrupolar fields distribution that have a minimum in the electric field in both z directions;

molecules that are in the high field seeking states. However, they can be focused in only one transverse direction, while being defocused in the other because, it is not possible to have a maximum in the electric field in both dimensions in free space.

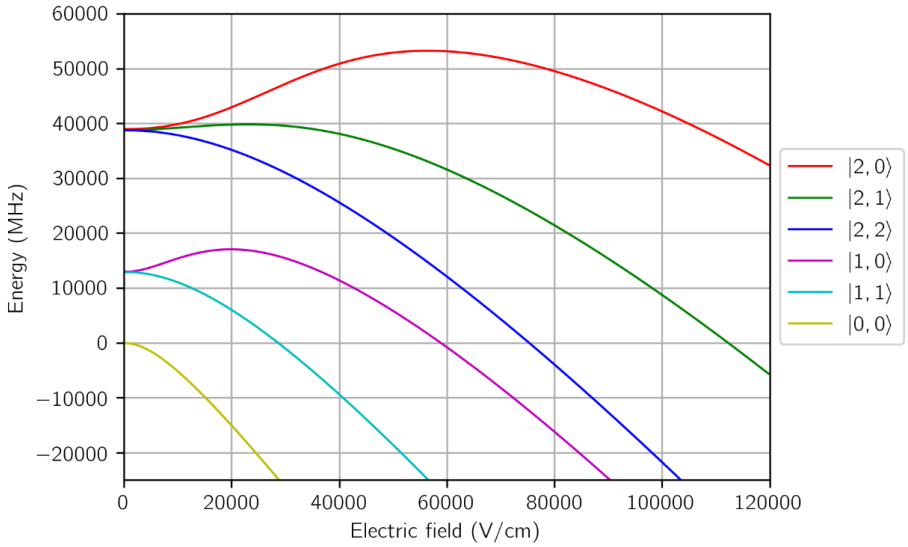

Figure 6: *This is the Stark shift for N = 0, 1, 2 levels in the ground state. The states are labeled as follow* $|N, |m_N|\rangle$. *This image is taken from the original source [19].*

If this were the only relations to the Stark shift than it would follow quadratic shifts in the electric field strengths, but it is never that simple. We can see from experiments and the simulations like Fig. 6. For higher electric field strengths, unfortunately the previous Hamiltonian is not enough. To solve this, far more difficult and larger Hamiltonian needs to be computed by PGOPHER:

$$H_{Full} = H_{sr} + H_{hfs} + H_{so} + H_{\Lambda d} + H_{rot} \tag{11}$$

Here $H_{\Lambda d}$ and H_{rot} are the Λ-doubling Hamiltonian and the rotational Hamiltonian, respectively. The rotational Hamiltonian is important in this because it plays a role in every electronic state. So, these calculations are done to discover the different levels of the Stark shift at given electric fields. Only $H_{\Lambda d}$ is not described above, therefore see the data gathered found [19]. These data points were then used by our simulations to make a fit function over them, this in order to extract the Stark shift of every given electric field, as discussed in section 3.1. So, with this method the Stark shift was acquired for the computational simulations.

2.4 Phase-Space

There has been a lot of talk about longitudinal and transversal velocities and about our molecules focusing on the decelerator. These subjects mix with each other in this especially important section. By now we have seen how the electric field behaves inside the guide and how particles react according to that. This will give the particles position and velocity at a certain time, which will be crucial for determining whether a particle will make it into the decelerator. If a particle has made it into the guide, its position is good but its velocity is too high, causing the particle to hit the electrodes. This can also work the other way around with the right velocity but wrong position. We can make an 2D or 3D representation of this, which is called position-momentum space or the Phase Space. In the decelerator, the control of the molecules comes from the manipulation of this phase space. Causing the particles to slow down and bunch together. More on how this is done can be seen in [20]. For our guide we want to match our phase space of the particles exiting, to the phase space of the low field region created by the decelerator. This matching of the phase space is referred to as the acceptance of the decelerator. To know where the acceptance is the largest for our guide design, we will look at the time evolution of the phase space. This will tell us how the motion of a group of molecules will evolve over time.

2.4.1 Liouville's Theorem

When the non-Hamiltonian forces do not depend on the velocity. Thus, when there is an absence of dissipative forces that would depend on the velocity and change the energy in the system. From this we can say that the phase space density will stay constant. This is the Liouville Theorem [21]. It states that in a system which is only acted upon by forces that can be derived form a potential, such as ours [22]. Which means that in a system with forces that will only depend on the position of the molecule, not on the velocity. This Liouville's theorem can therefore also be applied in time-varying electric fields like is proven in [23], and is done in [20] for our Stark decelerator.

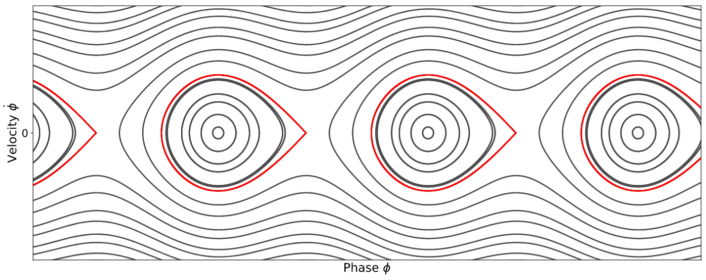

Figure 7: *The beautiful computer simulation of the Liouville's theorem done for the decelerator. More on this and the image where it is taken form the original source [20].*

From the Liouville's theorem two important properties of the phase space can be derived. As first, at any given time different trajectories in phase space will not intersect. This can be seen form the fact that in a Hamiltonian system, time and the initial conditions solely determine the resulting motion. Therefore, if trajectories would intersect, then they will have same position and momentum at that certain time and the resulting motion afterwards would be the same. As secondly, from the first property it follows that the motion of a group of molecules in phase space can be calculated if we track the boundary of a group in phase space. The group of molecules will behave as an incompressible fluid. Thus, its shape of its six-dimensional volume can change, but the volume itself cannot [24]. This can be seen in Figure 7.

2.4.2 Phase Space Matching

Because the phase space density cannot increase, it also cannot decrease. But it can be diluted, this happens when a group of particles is transferred from one element to the next. But these elements are not properly matched, such as can happen for our guided molecules and the phase space of the decelerator as is illustrated in Figure 8.

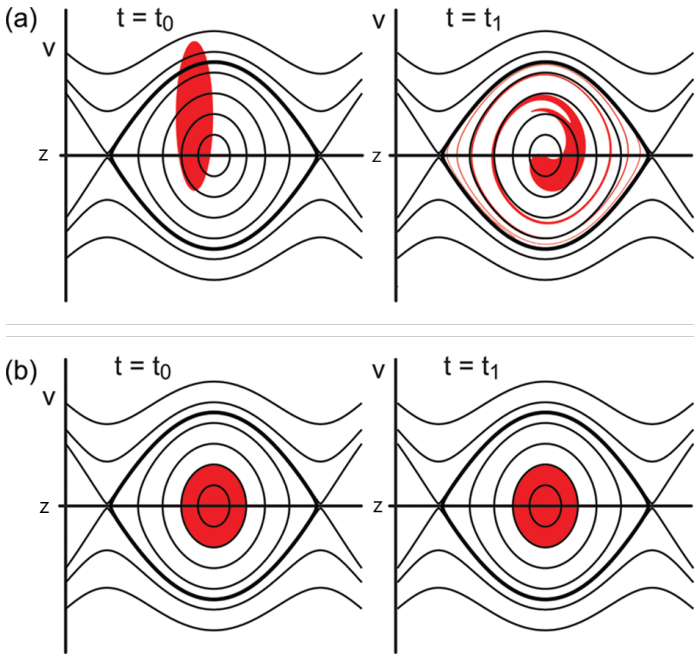

Figure 8: *Non-ideal (a) vs ideal (b) phase space matching. In this image it is clearly visible what happens when molecules are not perfectly within the right phase-space. This image is taken from the original source [11].*

In the figure you can see on the left side the situation just before the potential is switched on. On the right side you see the situation after the potential is switched on after a certain amount of time has passed. The red colored area illustrates the position and the velocity of a group of particles, but also known as the emittance of the beam, that is a number with units of $m \cdot \frac{m}{s}$. In this picture, the solid curves illustrate the lines where, potential + kinetic energy is equal. The Bold solid curve illustrates the outermost closed equipotential, called the separatrix. Particles within this area are in closed orbits in the phase space giving the molecules an oscillatory motion in real space and in momentum space. Therefore, they are kept together during the deceleration process in this phase space, also known as the acceptance. Molecules outside this area have a larger emittance of the molecular beam than the entering acceptance. These cannot be decelerated in a phase-stable manner, they will be cut off and lost from our original molecule beamline. If we look back at figure 8 now, there are three imperfections in the upper-left illustration.

1. The emittance of the particle beam is larger that the separatrix of the potential, thus particles will be lost.

2. The separatrix and the emittance are not centered around the same point, as a result the beam will oscillate back and forth in the potential, this will lead to phase space dilution.

3. The separatrix and the emittance do not have the same shape in phase space, this will lead to phase space dilution.

If we want to avoid all these imperfections, we need to shape the emittance properly, the so-called phase space matching. This is done in our instance with the hexapole. Such that the acceptance of the decelerator and the emittance of the molecular beam match.

2.4.3 Phase Space Transformations

If we look at the phase space transformations, we notice two general and important transformations. The translation we know as the linear free flight of a molecule in real space. The rotational, we know from when a linear force is applied to a molecule. From this you can notice that they both are linear in nature and this will become visible in the results section. Therefore, the transformations in phase space of the velocity and position coordinates can be expressed in a matrix notation. For simplicity's sake and reasons explained in the discussion, in our free flight sections no forces will act on the molecules. Therefore, in this region the velocity spread will be constant. The consequence of a free flight that has a velocity of v_z, doing this a time t will give the matrix notation:

$$\begin{pmatrix} z_f \\ v_{z_f} \end{pmatrix} = \begin{pmatrix} 1 & t \\ 0 & 1 \end{pmatrix} \begin{pmatrix} z_i \\ v_{z_i} \end{pmatrix} \tag{12}$$

In this the f and i stand for the final and initial state of the upper. If the molecules would only experience free flight than many molecules will be lost, as can be seen in Figure 9. In this representation of the phase space the black part is the entering beamline ($t = t_i$), the red part is the position and momentum of the molecules after the free flight in time ($t = t_f$). The green part is the acceptance of the decelerator, and thus from this you can see that the molecules that would be accepted into the decelerator diminish more over time.

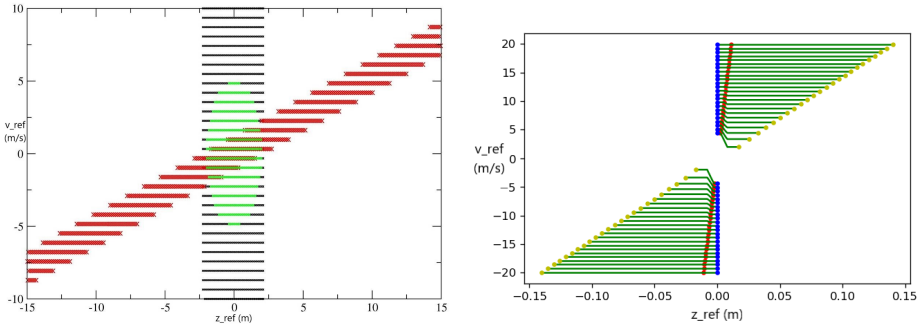

Figure 9: *Representation of phase space in free flight motion. The vertical axis gives the value for the velocity v_z. And the horizontal axis gives the position (z) with respect to the absolute values of the separatrix center. These images are taken from a simulation and the original source [25].*

If now our molecule beamline will experience a harmonic potential well with a linear force as a consequence applied to the molecule. This causes the position of the molecule to start to rotate in the phase space. The consequence of a linear force will give the change of the momentum and the position of the molecules. And this transformation will give the matrix rotation:

$$\begin{pmatrix} z_f \\ v_{z_f} \end{pmatrix} = \begin{pmatrix} cos(\omega t) & \frac{1}{\omega} sin(\omega t) \\ -\omega sin(\omega t) & cos(\omega t) \end{pmatrix} \begin{pmatrix} z_i \\ v_{z_i} \end{pmatrix} \tag{13}$$

For this situation, the rotation has a constant angular frequency ω. These phase space rotations are therefore used to keep the molecules within the phase space acceptance. In our setup however, it is difficult to have a perfect linear transformation. This is because the molecule experiences linear and quadratic forces and therefore the distribution does not rotate uniformly. The molecules further off the axis will rotate faster that the molecules close to our hexapole axis, as can be seen in Figure 10. This causes the phase space matching to be less desirable, as this will lead to the loss of phase space density.

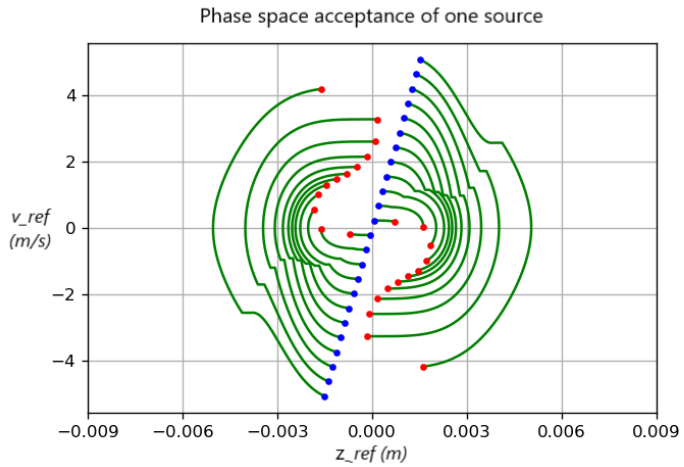

Figure 10: *Simple example of a simulation done where the vaster rotating properties is clearly visible.*

2.5 Loss Factor

To understand how much our guide will improve the acceptance of the Stark decelerator, two parameters are needed. These parameters will be referred to as the loss factor. If these values decrease then that means that the guide has a positive effect on the acceptance of the decelerator. Making the guides longer and then look at every applied voltage is the general solution for decreasing these factors.

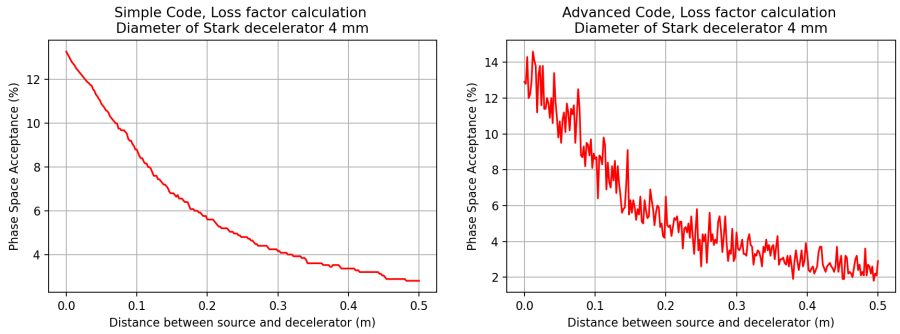

Figure 11: *On the horizontal axis the distance (m) between the hole of the source and the opening of the decelerator is denoted. On the vertical axis the acceptance as function of distance between source and decelerator is denoted. This is done both for the repaired/advanced Gauss distribution and for the simpler fan-like distribution.*

2.5.1 Overall Loss Factor

This will be the total amount of molecules created in a simulation, divided by the number of molecules in the correct phase space for deceleration. In Figure 11 the overall loss factor can be calculated for different distances between source and decelerator, with our any guide. For the current set-up, the distance between source and decelerator is 239 mm.

2.5.2 Guided Loss Factor

This will be the total amount of molecules that successfully reached the end of the guide in a simulation, divided by the number of molecules in the correct phase space for deceleration. So, this is very much like a success rate. This is especially useful for comparing individual cases.

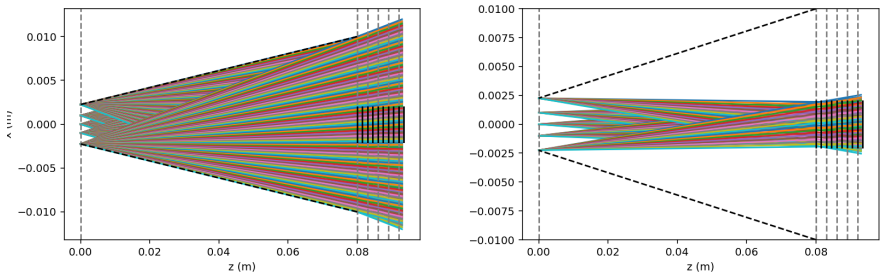

Figure 12: *Hypothetical situation if the distance between the source and the decelerator was zero. The black bars are the subsequently rings of the decelerator. For the measure above this distance is then increased to 50 cm. Left: All the molecules leaving the first hole ($2 \cdot r = 4.5$ mm) and fans over the second hole. Right: Same constants as on the left. But here only the trajectories of the molecules that make it into the first separatrix are depicted.*

2.6 Experimental Setup

In contrast to most Electrostatic hexapole/quadrupole using experiments, such as the spatial orientation of weak-field seeking and state-selecting focusing experiments. Our hexapole/quadrupole is designed to increase the BaF flux at the right acceptance at the beginning of the Stark decelerator. Also because of the size of the experiment, it is limited in its length. Therefore, the max length of the guide itself is around 500 mm. For the safety of our equipment we will leave 10 mm of space on each side of the guide, this is to prevent a discharge to the environment around the guide when the voltages on the guide become high, like ±12 kV. Also, from the decelerator 20 mm of space is left. This is larger because the electrodes of the decelerator are also charged. Therefore, making an electrical discharge more likely between the electrodes.

If our plan would be to place the guide in the exciting setup. Then we can determine that to the left of the valve there is about 124 mm off space we can use, out off the 134 mm. And on the right side of the valve there is at least place for a 60 mm long guide. These are both noticeably short guides and the hypothesis is therefore that the set-up needs to be extended. This is needed in order to have the guides do enough focusing of the molecule beams.

Furthermore, from the top figure 14, it is visible that the inner diameter is of 63 mm diameter. So, with the 10 mm of space from sides this leaves us with 43 mm. From earlier we know the desired rod radius, of the hexapole, is $0.565r_0$. So, our max inner radius of the hexapole can be calculated: $4 \cdot 0.565r_0 + 2r_0 = 43$ mm $\rightarrow r_0 \approx 10$ mm. The efficiency effects might not be significant enough for us to construct such a hexapole. It is even more possible that due to the enlarged radius the voltages needed for the best stark shift is out of the 12 kV limit.

The simulations will research the effects from 4 mm inner radius up to 10 mm inner radius, for both the hexapole and the quadrupole. Furthermore, it is probably much more efficient to extend the space for our guide on the rear or on the front. From the bottom Figure 14, it is visible there is room for this extension to be added to the setup. And from the talks with the experiment's supervisor, it is possible 50 cm might be added. Therefore, we will extent the rear guide to 50 cm in our simulations in section 4.4. And the front guide will be extended to 50 cm in our simulations in section 4.3.

Within the cryogenic source there is another hole were the molecules must first pass through. This hole has a diameter of 4.5 mm and is at a distance of roughly 80 mm from our second hole as can be seen in Figure 13. As mentioned before this second hole has a diameter of 20 mm.

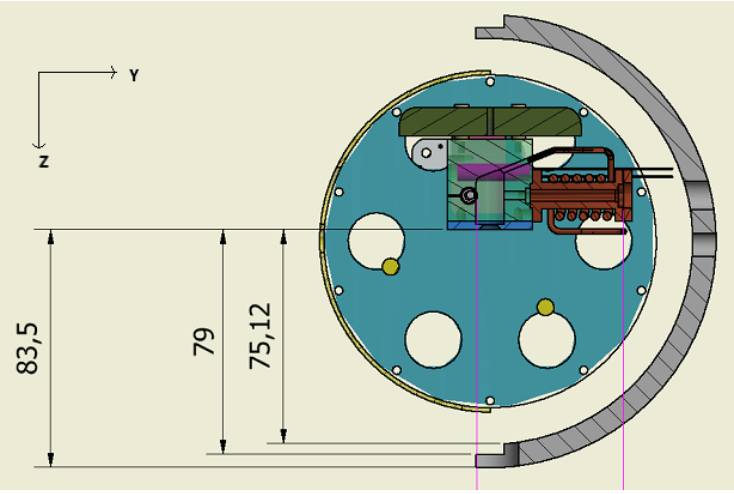

Figure 13: *Top view of only the cryogenic source with its shield at roughly 80 mm [26].*

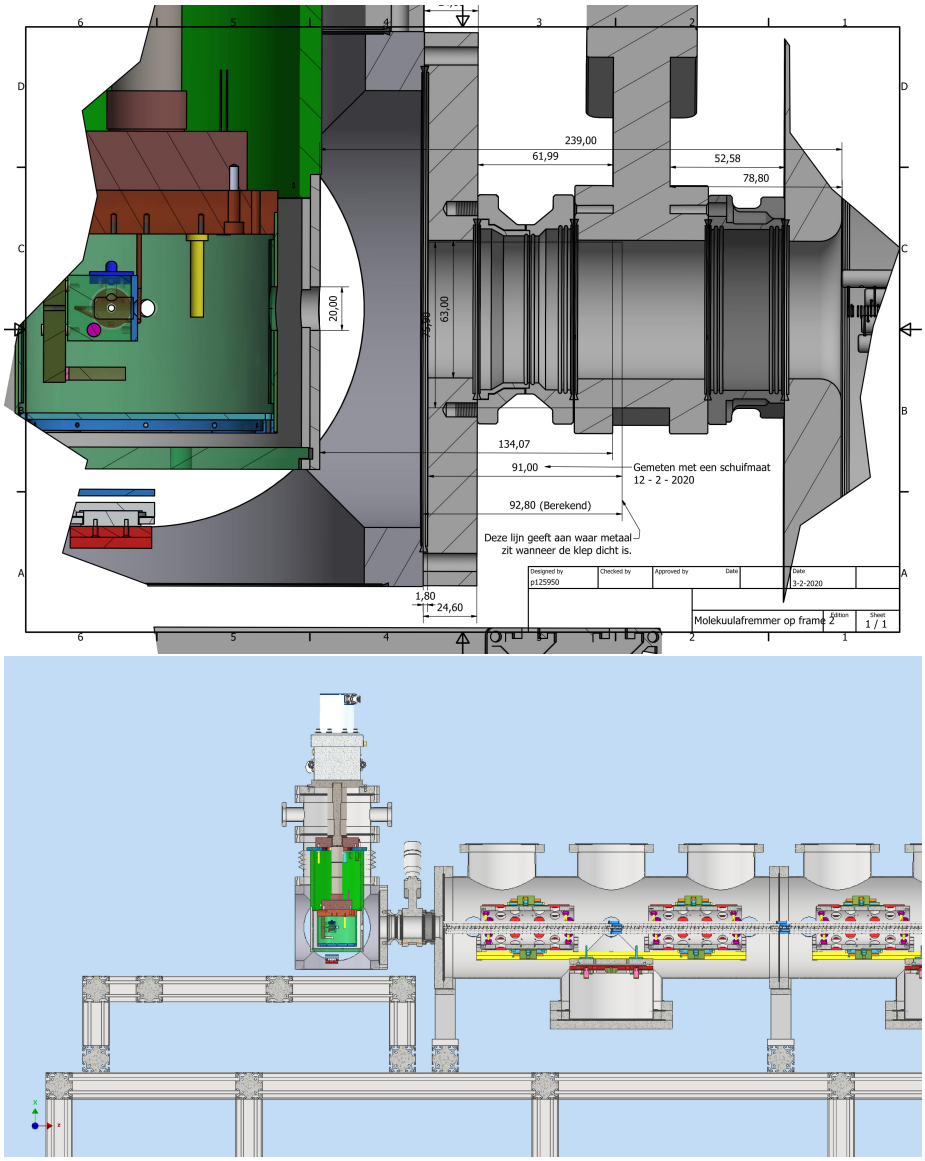

Figure 14: *Top: Detailed depiction of the cryogenic source on the left with the valve in the middle and Stark decelerator on the right. Bottom: Cryogenic source on the left and decelerator on the right. From here you can see that the cryogenic source has enough room to be moved more to the left [27].*

3 Computational Simulations

The terms Front and Rear guide come from the fact that there is a valve installed in the experimental setup. This valve allows the cryogenic source and decelerator to be sealed off from each other when this is needed. Such as during maintenance or when adjustments need to be made to either side of the valve. During which you do not want to be losing the vacuumlike pressures on the other side or let water into the vacuum chamber. Therefore, the Front guide will refer to the guide after the cryogenic source and before the valve. And the Rear guide will be the guide after the valve and before the decelerator.

The goal of the guide(s) is to catch as many BaF molecules coming out of the cryogenic source and focus them into the decelerator's acceptance. Here must be thought of the longitudinal velocities and the transverse velocities of every single molecule leaving the cryogenic source. The maximum applied voltages allowed to the rods is ±12 kV. The longitudinal velocities (v_l) and the transverse velocities (v_t) of the molecules leaving the cryogenic source measured by my colleagues are respectively, $v_l = 195 \pm 5$ m/s and $v_t = 0 \pm 50$ m/s. If the guides are not turned on, the loss factors of how many not make it into the decelerator's acceptance is exceptionally low. For the fan distribution only 3.44% make it into the decelerators acceptance of all the molecules created, this is then a loss factor of 29.

3.1 Fit Function

In order to calculate the stark shift for our particles that are in the guide, the data gathered by PGOPHER of the lowest rotational levels in the ground state is used [19]. With this data a fit function can be made which perfectly coincides with the theoretical function for stark shift versus electric field. The fit function plotted in Figure 15 is one of the Stark shift lines from figure 6, this particular plot gives the $|N, m_N\rangle = |10\rangle$ state. This state is preferred to be guided properly, because this quantum level is very well decelerated in the Stark decelerator.

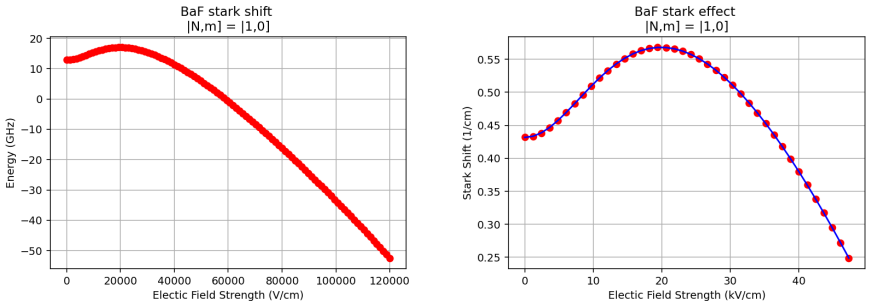

Figure 15: Left: Full data set of $|10\rangle$ from the master thesis [19]. Right: The fit over the data that is relevant for our guide strengths.

From figure 6 the data can be used to also graph the $|N, m_N\rangle = |20\rangle$ state. This state is also very desirable to use for the deceleration process and was therefore also planned to be tested. Unfortunately the there was no time left for anymore simulations after the delivery of the data. Most of the code is written so the NL-eEDM team can proceed with testing this state if that is desired. The fit function for this state is plotted in Figure 16.

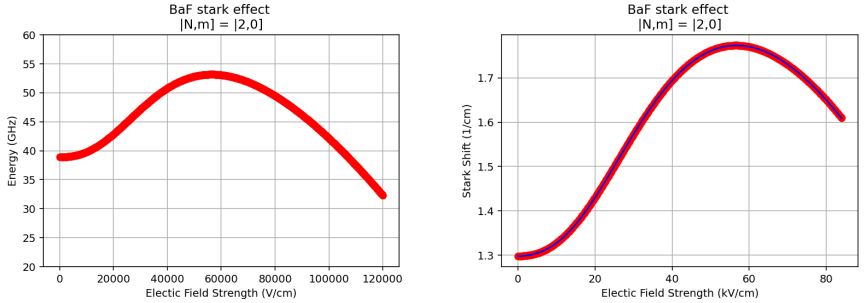

Figure 16: Left: Full data set of $|20\rangle$ from the master thesis [19]. Right: The fit over the data that is relevant for our guide strengths.

3.2 Sanity Check

In order to check if the results follow the theory, we must first preform a sanity check [25]. This check is done by making the problem slightly simpler. We will only consider the linear forces acting on the particle. With this we can now calculate the theoretical electric field strengths, Stark effect, oscillation frequency (ω in Eq. 14) and wavelength (λ in Eq. 15) [22][25], and compare this with the simulated focus point of the molecules that experiences the same conditions as used in the calculations. We use focus point here because if the effects are only linear the guide will work like a lens. This check will be done for the hexapole and the quadrupole case. And from the calculation below we can conclude that the code coincides with the theory. So now we can add the quadratic effect and know the gotten results are a representation of the reality.

$$\begin{aligned} \omega_{hexapole} &= \frac{1}{2\pi}\sqrt{\left(\frac{-3\mu_{eff}V}{M\ r_0^3}\right)} \approx 158.2Hz \\ \omega_{quadrupole} &= \frac{1}{2\pi}\sqrt{\left(\frac{2\alpha}{M}\left(\frac{V}{r_0^2}\right)^2\right)} \approx 193.3Hz \end{aligned} \tag{14}$$

$$\begin{aligned} \lambda_{hexapole} &= \frac{v_l(=200m/s)}{\omega_{hexapole}} \Rightarrow \frac{\lambda_{hexapole}}{2} \approx 0.632m \\ \lambda_{quadrupole} &= \frac{v_l(=200m/s)}{\omega_{quadrupole}} \Rightarrow \frac{\lambda_{quadrupole}}{2} \approx 0.517m \end{aligned} \tag{15}$$

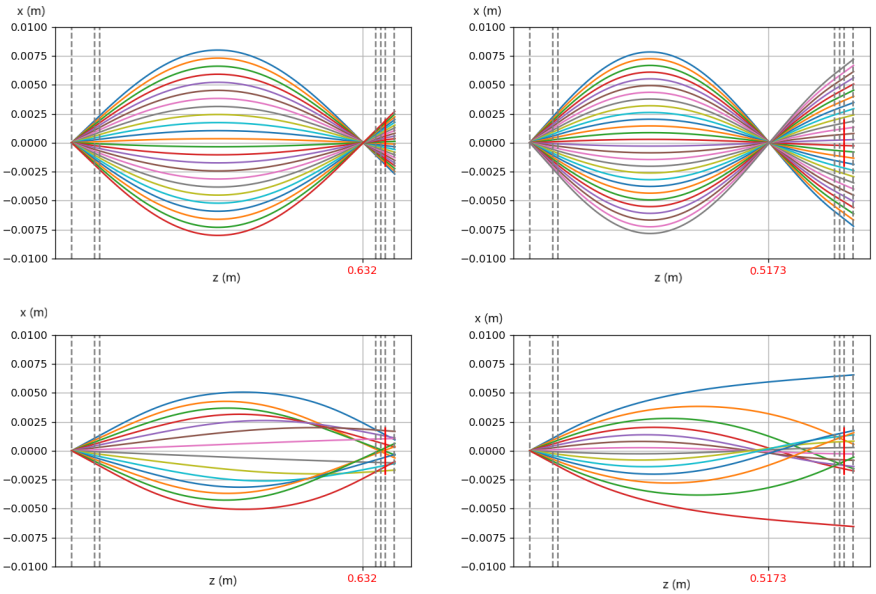

Figure 17: Left: Hexapole prove for only linear forces acting on the particle. And below the hexapole with the same conditions, but with the quadratic effect. Right: quadrupole prove for only linear forces acting on the particle. And below the quadrupole with the same conditions, but with the quadratic effect.

3.3 Source Creation

The code that calculates the trajectories of the particles is made in such a way that with minimal adjustment all sorts of distributions of molecules can be tested. Therefore, the gotten results from the tests done on the distribution leaving the cryogenic source, can be implemented here. Which is useful for further research the NL-eEDM team wants to do. How interesting this may be, this will surpass the goal of this thesis. The code used to generate the source is made in such a way that the effects of the different longitudinal and transversal velocities are better visible. Therefore, making the understanding and experimenting with the actual physics involved a more centerpiece of the code. And optimizing this first is than more significant for this thesis, before you start adding noise and uneven distributions.

Thus, the distribution used is a 'fan' like distribution. This fan made in such a way that the transversal and longitudinal velocities match with that of the molecules form the source. They will all go trough the opening in the cryogenic source and they will originate from five point. This is done to still have the desirable properties of the fan, but still have a nonuniform distribution. An example is shown in Figure 18. In this figure on the left: The trajectories are simulated for all the molecules that make it to the end of the guide. And on

the right just all the molecular trajectories that are calculated are depicted. Quick side-note, here is some beautiful example of the chaos theory visible on the right.

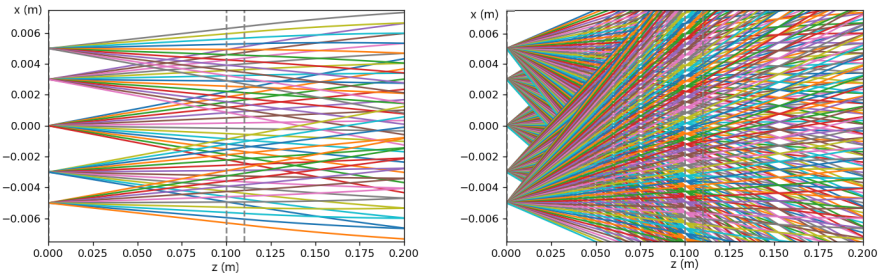

Figure 18: Both: Just an example of how this might look. In Fig. 12 more accurate depiction. Left: The trajectories of particles make it to the end of the guide Right: The trajectories of all the particles from the same example.

4 Simple Code Computational Simulation

4.1 Differences Between Codes

After some further investigation into more Python code a more accurate representation was found for the simulation. In earlier results the computation would take up to six hours to create three small graphs. So, improvement was made to make it faster, now the code does not have to calculate the derivative by itself, but it is done beforehand. Therefore, the applied voltages can be measure with tinier intervals between another. With this, decreasing the errors margin in the graphs. Also, from communications with the NL-eEDM team, it was deducted what range of particle make it out of the source [26].

Of the particles generated in the source a lot do not reach the outside of the source, due to its transversal velocities and the geometry of the source. So, the transversal velocities are limited by $v_t = 25\ m/s$. Due to the first hole which has a diameter of 4.5 mm. This will cause the previous wide range of transversal velocities to be seriously diminished. Now we have to redo a few simulations. All the sections till section 5, have been redone. Sadly, no more time was left to implement these changes further. The results after this are precise but take more molecules in consideration that never could have reached the outside of the source. "Luckily" these are also the molecules that have such a high transversal velocity, that they could not be guided properly. So, in short, the values from section 5 are lower because of additional transversal velocities, but they are correct and therefore still interesting.

4.2 Front Guide Results

Placing a guide, but only in front of the valve is the simplest to do of all three options. This is because the placing of a Rear guide is more difficult than a Front guide as will be explained in section 4.4. It also makes a lot more sense in terms of what the effective goal of the guide is. Therefore, a large range of simulations will be done on this particle topic. Due to the transverse velocities of the molecules leaving the source, placing only a Rear guide can result in losing many molecules that wont even reach the guide. The geometry of this guide is such that 10 mm of space is between the guide and the cryogenic source to prevent an electrical discharge between one another. The effective length can be 125 mm, this leaves 2 mm space between the guide and the valve if it is closed. Therefore, the distance between the valve and the cryogenic source is 137 mm and the decelerator are 239 mm from the cryogenic source as can be seen in Figure 14. In section 4.3, we look at the effects when this guide is extended.

4.2.1 Radius Effects Hexapole

The effect of different inner radius of the hexapole front guide is tested for different applied voltages. The graphs will then give the quantity of the molecules which are guided correctly within the decelerator in the correct phase space of (± 5 m/s) transversal velocity for different applied voltages and correct (± 3 mm) longitudinal distance from the separatrix center. From Figure 20 it is concluded that the 4 mm inner radius gives the highest acceptance of 6.2% at 6.5 kV. This is a decrease of the overall loss factor to roughly 16.1, from 29. Which are respectable results. Furthermore 532 molecules are guided successfully and therefrom 310 molecules reach the stable space phase for deceleration. 58,3% is successfully phase space matched, thus a guided loss factor of 1.7.

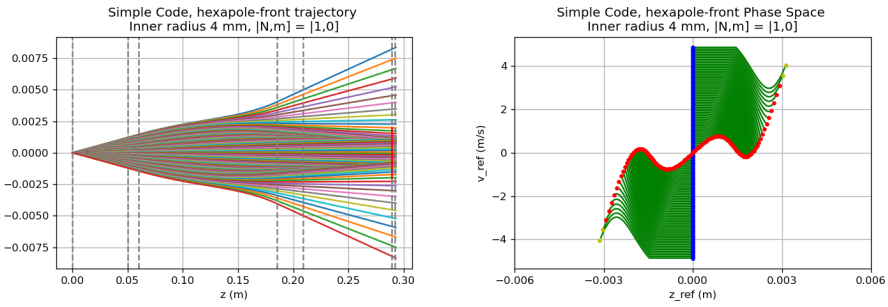

Figure 19: Left: The trajectories of the successfully guided molecules. Right: The phase space transformation of the guided particles for 6.5 kV voltage. Blue dots are the starting positions in phase space. After that, the free flight before guiding is clearly visible.

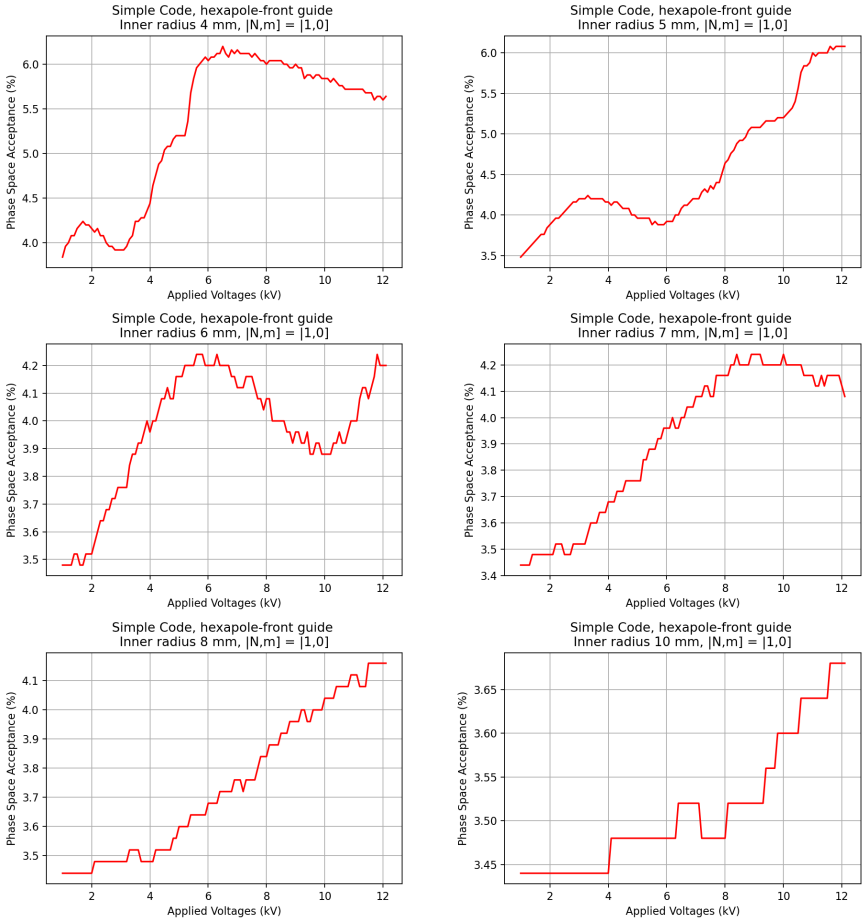

Figure 20: Decelerators acceptance of the guided molecules for different applied voltages (kV) at different radii at the vertical axis. 5000 molecules are generated per applied voltage with steps of 0.1 kV

4.2.2 Phase Space Acceptance in the hexapole lens

From Figure 20 it is visible that a radius of 4 mm gives the highest acceptance. Let us look at the phase space of the 4 mm case for only our middle source, otherwise the phase space plot becomes complicated. In Figure 19 the phase matching of the molecules further away from the axis is much better than those molecules close to it. As you could expect from the theory.

4.2.3 Radius Effects Quadrupole Lens

It is suspected that a (relatively) short hexapole has not as much effect as a short quadrupole. Because for shorter distances the molecules closest to the axis, have

the highest chance to be "pushed" into the right acceptance. Hexapoles tend to work better for molecules further from the axis. Therefore, the same test is done for the quadrupole to see the differences. Again the graph will then give the quantity of the molecules which are guided correctly within the decelerator in the correct phase space of (± 5 m/s) transversal velocity for different applied voltages and correct (± 3 mm) longitudinal distance from the separatrix center.

From Figure 21 it is concluded that 4-6 mm inner radii give the highest acceptance of 5.6%. This is a decrease of the overall loss factor to roughly 17.9, from 29. Which are respectable results but not as good as the hexapole. Furthermore 578-798 molecules are guided properly and therefrom 280 molecules reach the stable space phase for deceleration. Thus 48.4-35.1% is successfully phase space matched. And with that guided loss factors of 2.1-2.9.

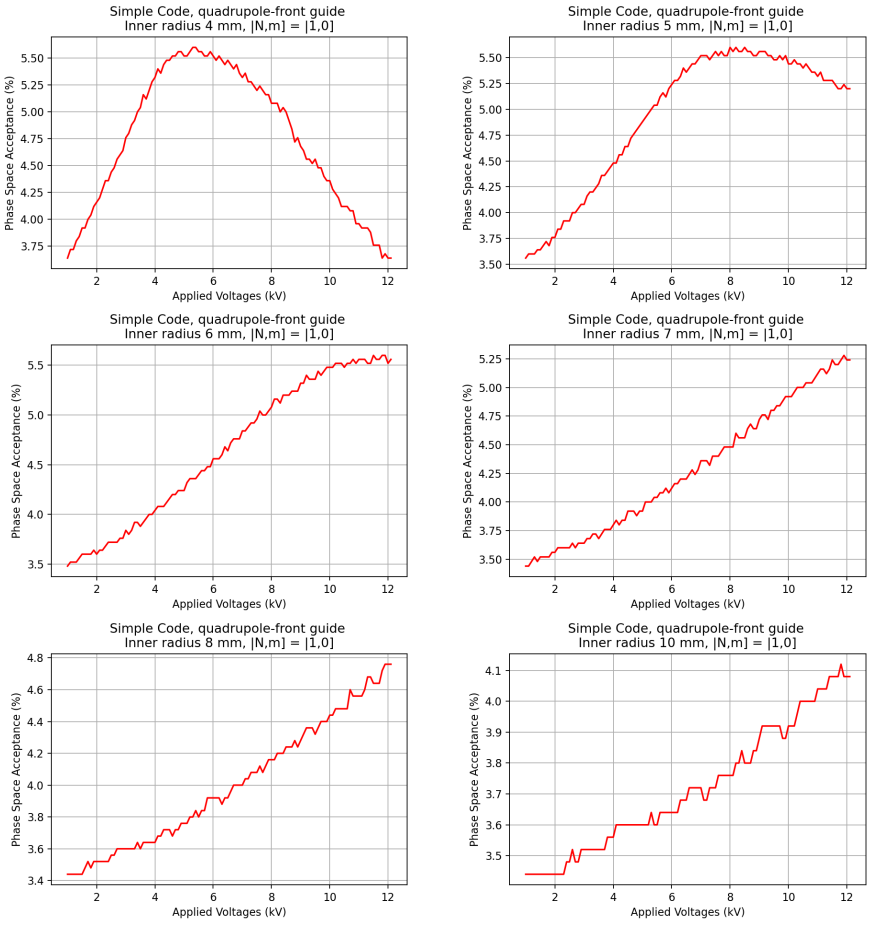

Figure 21: Decelerators acceptance of the guided molecules for different applied voltages (kV) at different radii at the vertical axis. 5000 molecules are generated per applied voltage. With steps of 0.1 kV.

4.2.4 Phase Space Acceptance in an Quadrupole Lens

From Figure 21 it is visible that if we were to switch to a quadrupole instate of an hexapole, it will result in a small decrease in the acceptance. To understand why, lets look at the phase space of the 4 mm case. Again, just for our middle source, otherwise the phase space plot becomes too complicated to understand. From the graphs you can see that the molecules close to the axis are guided better than those in the hexapole. But further away from the axis the hexapole is more effective. This is precisely what was hypothesized.

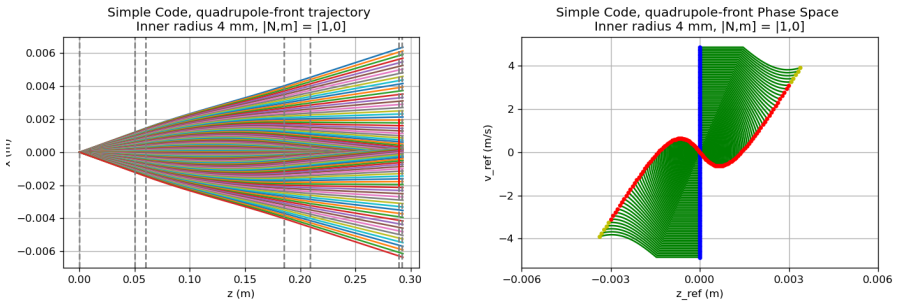

Figure 22: Left: The trajectories of the properly guided molecules. Right: The phase space of the guided particles for 5.4 kV voltage.

4.3 50 cm Long Front Guide Results

The same is done as above but now the front guide is extended to 50 cm to look at these effects. The geometry of this guide is such that 10 mm of space is between the guide and the cryogenic source to prevent an electrical discharge between one another.

4.3.1 Radius Effects Hexapole

The effect of different inner radius of the long hexapole front guide is tested for different applied voltages. The graphs will then give the quantity of the molecules which are guided correctly within the decelerator in the correct phase space of (±5 m/s) transversal velocity for different applied voltages and correct (±3 mm) longitudinal distance from the separatrix center.

From Figure 23 it is concluded that the inner radii of 6-8 mm give the highest acceptance of 5.76%. This is a decrease of the overall loss factor to roughly 17.4, from 29. Which are respectable results but remarkably, the shorter guide had a better acceptance.

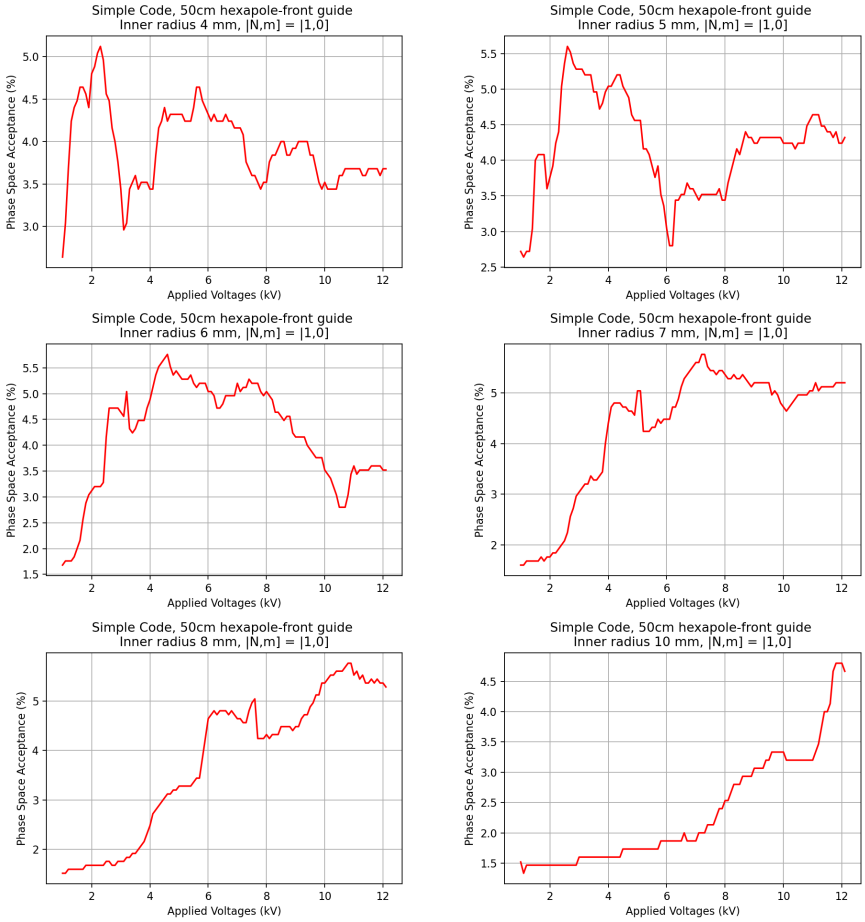

Figure 23: Decelerators acceptance of the guided molecules for different applied voltages (kV) at different radii at the vertical axis. 5000 molecules are generated per applied voltage with steps of 0.1 kV. From radius 4 mm to 10 mm, the following guided loss factor was found: 1.71, 1.78, 1.81, 1.83, 1.88 & 2.63, respectively.

4.3.2 Phase Space Acceptance in the hexapole guide

From Figure 23 it is visible that three radii gave the highest acceptance. Resulting in the next graphs in Figure 24. In the top two figures, let's look at the phase space of the 7 mm case for only our middle source, otherwise the phase space plot becomes complicated. At the bottom two, the same situation occurs but then with the additional sources turned on.

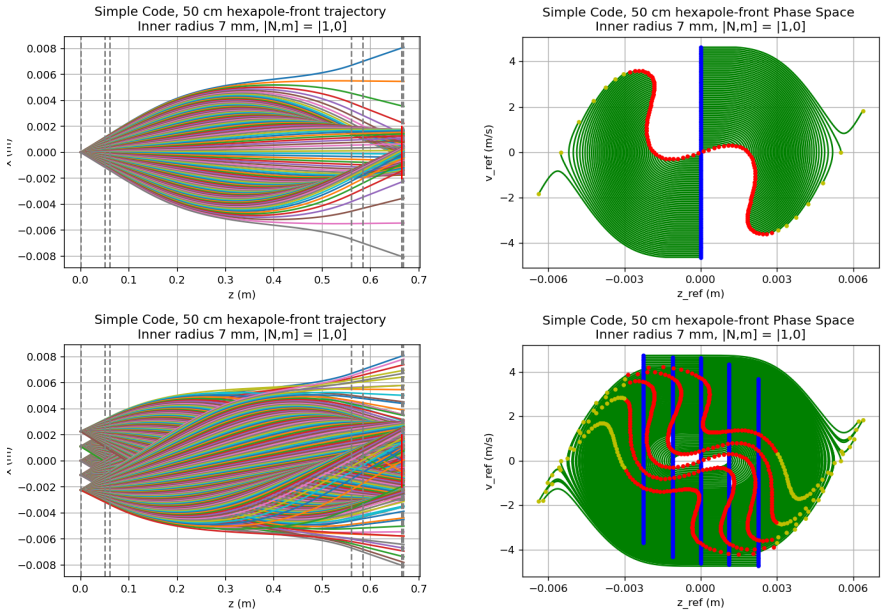

Figure 24: Left: The trajectories of the successfully guided molecules. Right: The phase space transformation of the guided particles for 7.2 kV voltage.

4.3.3 Radius Effects Quadrupole guide

Again the graph will then give the quantity of the molecules which are guided correctly within the decelerator in the correct phase space of (±5 m/s) transversal velocity for different applied voltages and correct (±3 mm) longitudinal distance from the separatrix center.

From Figure 25 it is concluded that 5-8 mm inner radii gives the highest acceptance of 5.04%. This is a decrease of the overall loss factor to roughly 19.8, from 29. Which are respectable results but not as good as the hexapole.

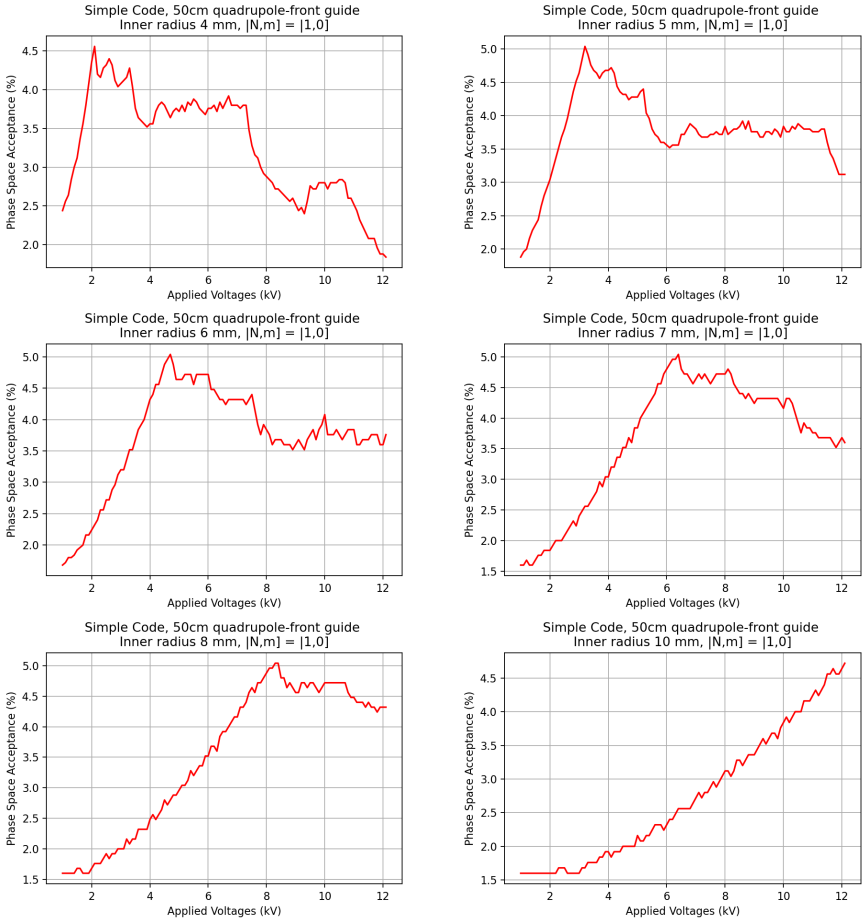

Figure 25: Decelerators acceptance of the guided molecules for different applied voltages (kV) at different radii at the vertical axis. 5000 molecules are generated per applied voltage. With steps of 0.1 kV. From radius 4 mm to 10 mm, the following guided loss factor was found: 1.46, 1.64, 1.86, 2.02, 2.13 & 2.58, respectively.

4.4 Rear Guide Results

Only placing a guide behind the valve is more complex than a Front guide and less effective. However, this information is particularly useful for the design of the most desired simulation, a front and rear guide as mentioned in section 5.1. The rear guide is more difficult to be installed into the experimental setup due to the mounting of high voltage wiring. The geometry of this guide is placed 20 mm from the decelerator to prevent an electrical discharge between the electrodes from the guide and the electrodes of the decelerator. And then it has the same 2 mm of space between the guide and the valve. The length of

this guide is not determined yet, but it can be at least 60 mm to an maximum of 500 mm as is done in section 4.5 and is discussed in section 2.6.

4.5 50 cm Long Rear Guide Results

The same is done as above but now the rear guide is extended to 50 cm to look at these effects. The geometry of this guide is such that 20 mm of space is between the guide and the Stark decelerator to prevent an electrical discharge between one another.

4.5.1 Radius Effects Hexapole

The same function is displayed on the vertical and horizontal axis as before. From Figure 27 it is concluded that the 7 mm inner radius gives the highest acceptance of 5.84% at 5.6 kV. This is a decrease of the overall loss factor to roughly 17.1, from 29. Which are respectable results and remarkably just slightly lower than the front long hexapole. Furthermore 440 molecules are guided successfully and from that 292 molecules reach the stable space phase for deceleration. 66,4% is successfully phase space matched, thus a guided loss factor of 1.5.

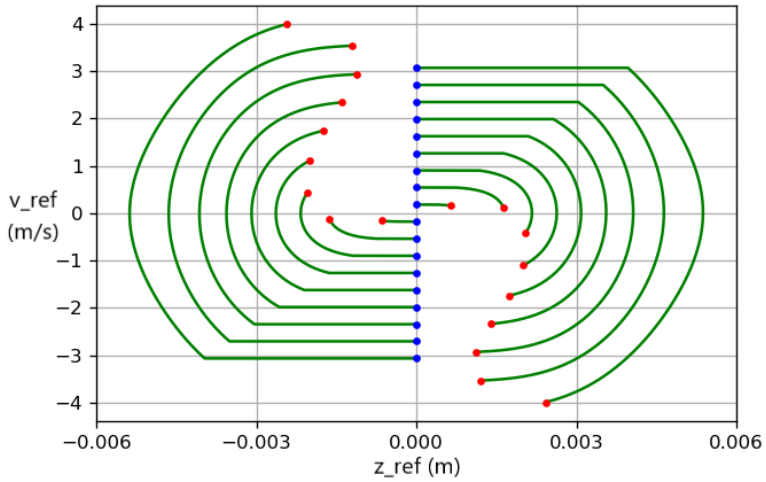

Figure 26: *This shows the phase space transformation of the long rear guide for one source. Blue dots are the phase-space position how they are created and the red dots is where they end up.*

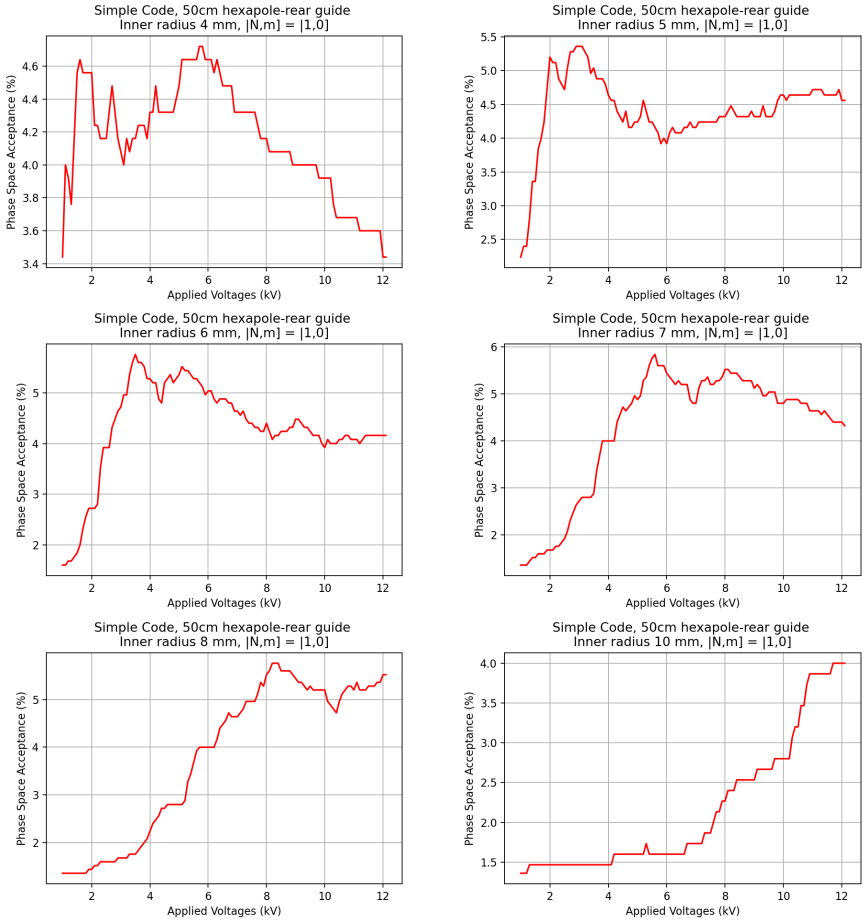

Figure 27: Decelerators' acceptance of the guided molecules for different applied voltages (kV) at different radii at the vertical axis. 5000 molecules are generated per applied voltage with steps of 0.1 kV. From radius 4 mm to 10 mm, the following guided loss factors were found: 1.05, 1.45, 1.49, 1.51, 1.54 & 2.43, respectively.

4.5.2 Radius Effects Quadrupole

The effect of different inner radius of the long quadrupole rear guide is tested for different applied voltages. Same quantities are represented in the graphs. From Figure 28 it is concluded that the 5-8 mm inner radii give the highest acceptance of 5.04%. This is a decrease of the overall loss factor to roughly 19.8, from 29. Which are respectable results and it is noticed that this is precisely the same as the short quadrupole front guide and their acceptance is worse than the hexapoles'.

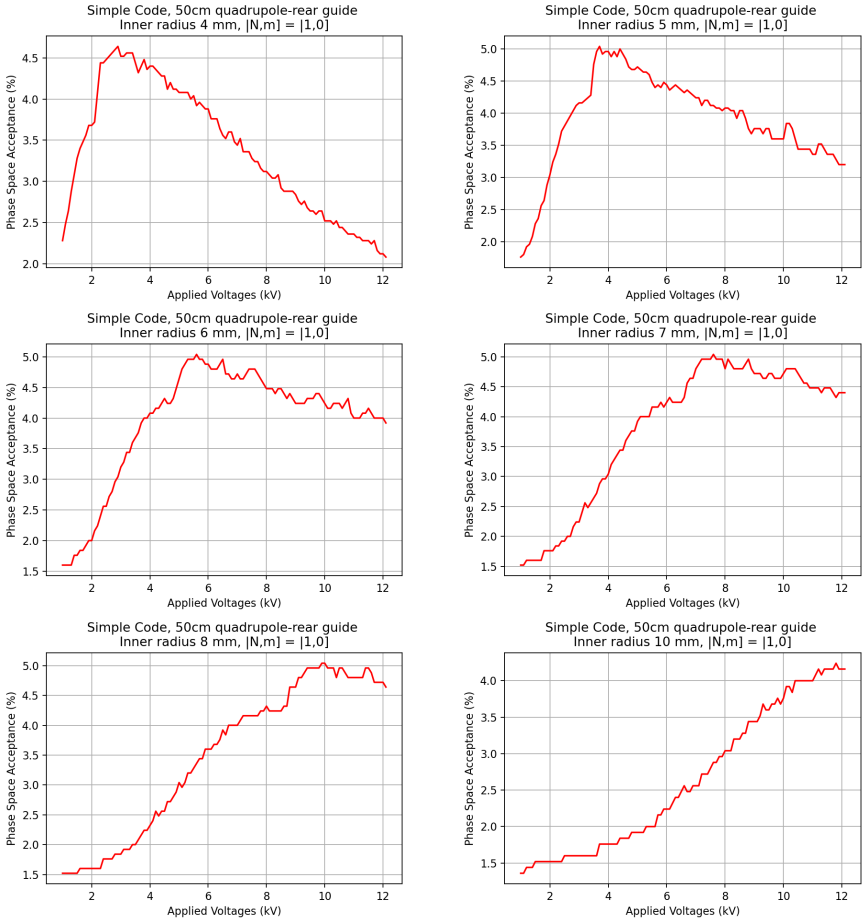

Figure 28: Decelerators acceptance of the guided molecules for different applied voltages (kV) at different radii at the vertical axis. 5000 molecules are generated per applied voltage with steps of 0.1 kV. From radius 4 mm to 10 mm, the following guided loss factors were found: 1.32, 1.38, 1.49, 1.54, 1.57 & 2.27, respectively.

4.6 Combining Front and Rear Guide Results

From all the sections above it can be concluded that a hexapole front and a 50 cm hexapole rear guide will give the highest acceptance. Therefore, the front guide at 4 mm with 6.5 kV applied will be tested for different long rear guides. The rear guide will only be tested up to 8 mm because the 10 mm never gave a better acceptance in any situation. Furthermore the 3 mm case is added, from Figure 29 it is visible why this might be interesting. This could focus these last molecules on the outside further inwards. For the results, the guided loss factor is precise, so we need to switch to percentages instead of loss factors. So, these percentages show how many of the molecules that reach the end of the guide are also found in the right space phase to be decelerated. Thus, the molecules that are guided successfully and are within the acceptance of the decelerator.

From radius 3 mm to 8 mm, the following percentages guided to stable were found: 99.3%, 99.1%, 84.4%, 84.4%, 84.4% & 76.5%, respectively. The highest overall acceptance was measured at 11.4% for the radii of 4-7 mm. This is therefore a decrease of the overall loss factor from 29 to 8.8. Thus, the loss can be decreased with a factor of 3.3 with this configuration.

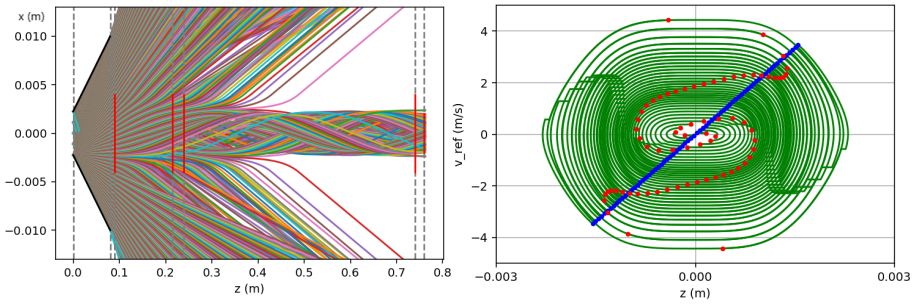

Figure 29: *Left: A depiction of the configuration with the best acceptance and highest guided percentage. So, the 4 mm front and 4 mm rear guide with 6.5 kV applied and with 6.9 kV applied, respectively. The red lines are the diameters of the guides and the decelerators entrance. Right: The phase space matching of this configuration for one source turned on.*

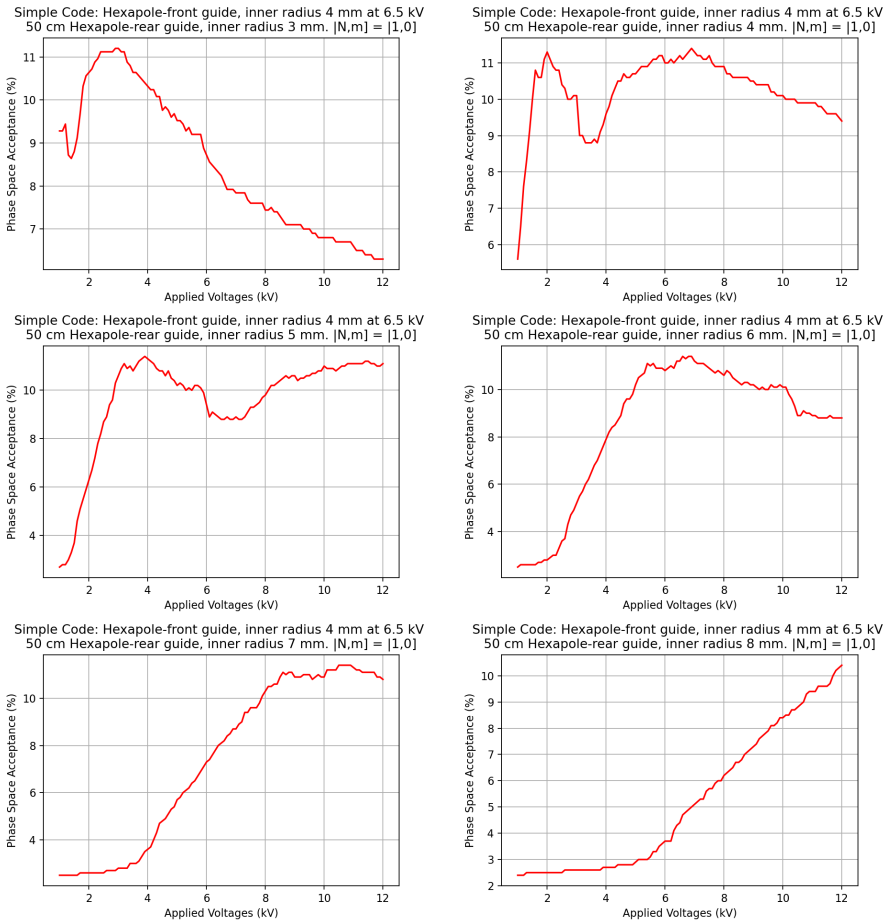

Figure 30: Decelerators acceptance of the guided molecules for different applied voltages (kV) at different radii at the vertical axis. 2000 molecules are generated per applied voltage with steps of 0.1 kV. From radius 3 mm to 8 mm, the following guided loss factors was found: 1.01, 1.01, 1.18, 1.18, 1.18 & 1.31, respectively.

5 Slow Code Computational Simulations

5.1 Combining Front and Rear Guide Results

The achieved results from earlier done simulations for the Front and Rear guide, are combined. These are the situations when the transversal velocities were increased. With these results a good starting point was made to construct the design of two hexapole guides with different applied voltages. The other important part of this Rear guide is that it can have a different geometry than the front guide so a hexapole and quadrupole combined guide with different applied voltages. Both types of guides are examined in the simulation, because the different effects they have on the phase space matching are not to be underestimated. The quadrupole guide causes the phase space to have a good matching close to the axis part and the hexapole causes a good matching far from the axis. Let us look at some cases that might show to be interesting in section 5.1.1 & 5.1.2.

5.1.1 Quadrupole Front Guide and Hexapole Rear Guide

Again the graph will then give the quantity of the molecules which are guided correctly within the decelerator in the correct phase space of ($\pm$5 m/s) transversal velocity for different applied voltages and correct ($\pm$3 mm) longitudinal distance from the separatrix center.

The quadrupole front guides with radii 4-6 mm are the radii that gave the highest and same acceptance. The 6 mm is choice here as it has less molecules hitting the electrodes, these molecules may be guided in to the separatrix by the rear guide.

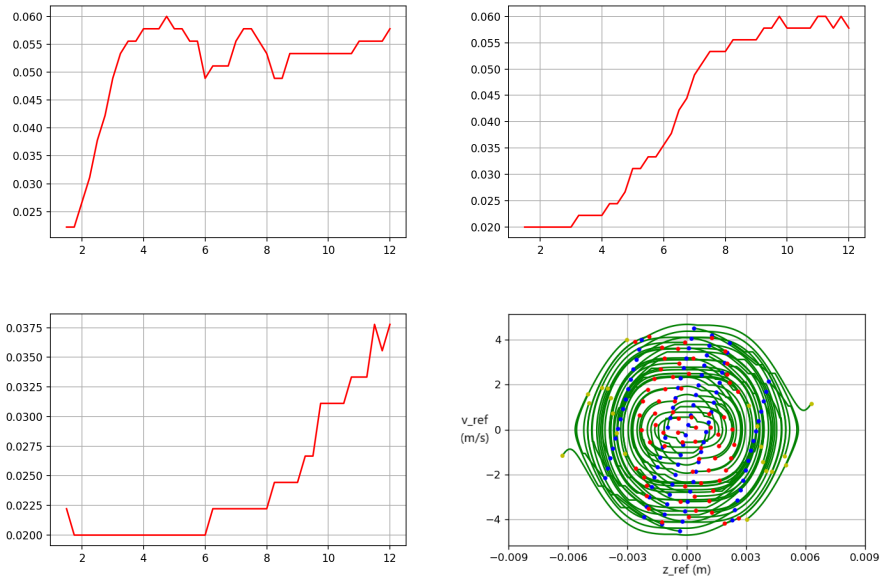

Figure 31: Per applied voltage to the rear guide 900 particles are generated for these graphs. Left: Decelerators acceptance of the guided molecules for different applied voltages (kV) with inner radius of 6 mm. Max acceptance: 6.0% at applied voltages of 4.75 kV. Below that, Decelerators acceptance of the guided molecules for different applied voltages (kV) with inner radius of 10 mm. Max acceptance: 3.78% at applied voltages of 11.5-12 kV. Right: Decelerators acceptance of the guided molecules for different applied voltages (kV) with inner radius of 8 mm. Max acceptance: 6.0% at applied voltages of 9.75∼12 kV. Below that, we see the phase space transformation of the 6.0% of the 8 mm case.

5.1.2 Hexapole Front and Quadrupole Rear Guide

Now perform a check that if the Rear guide is a quadrupole, the acceptance of the decelerator is actually better. Therefor the same simulations are done as seen above, but now with a 4 mm radius hexapole as front guide, and the rear guide is a quadrupole of inner radius of 4, 6 & 8 mm. The 10 mm radius will not be tested again. This is because in none of the simulations done before a higher acceptance was achieved with this radius. Plus, making these plots costs six hours. From Figure 32 we see that this is much lower than the previous case.

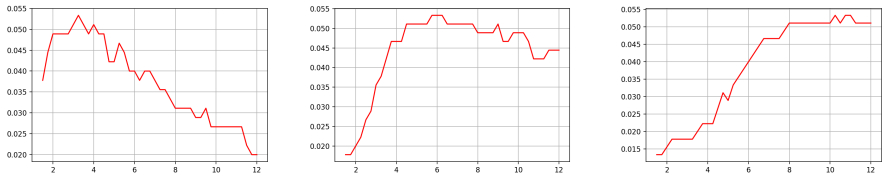

Figure 32: Per applied voltage to the rear guide 900 particles are generated for these graphs. Left: Decelerators acceptance of the guided molecules for different applied voltages (kV) with inner radius of 4 mm. Max acceptance: 5.33% at applied voltages of 3.25 kV. Middle: Decelerators acceptance of the guided molecules for different applied voltages (kV) with inner radius of 6 mm. Max acceptance: 5.33% at applied voltages of 5.75-6.25 kV. Right: Decelerators acceptance of the guided molecules for different applied voltages (kV) with inner radius of 8 mm. Max acceptance: 5.33% at applied voltages of 10.25∼11 kV.

5.1.3 Hexapole Front and Rear Guide

From section 4.5.1 & 4.5.1 it is clear that a hexapole front and rear guide is also remarkably interesting. Therefore, the same simulations are done as seen above, but now with an hexapole as front guide again. The rear guide is kept at the 8 mm standard inner radius as can be seen in Fig. 31 at 9.75 kV, as this gives max. acceptance.

From Figure 33 we see the highest achieved acceptance yet, at an impressive 7.78%. This displays the case for two hexapoles with the front one having the radius of 4 mm and the rear guide having the radius of 8 mm. This is an overall loss factor decrease from 29 to 12.9. So, it was decreased by two times and a quarter.

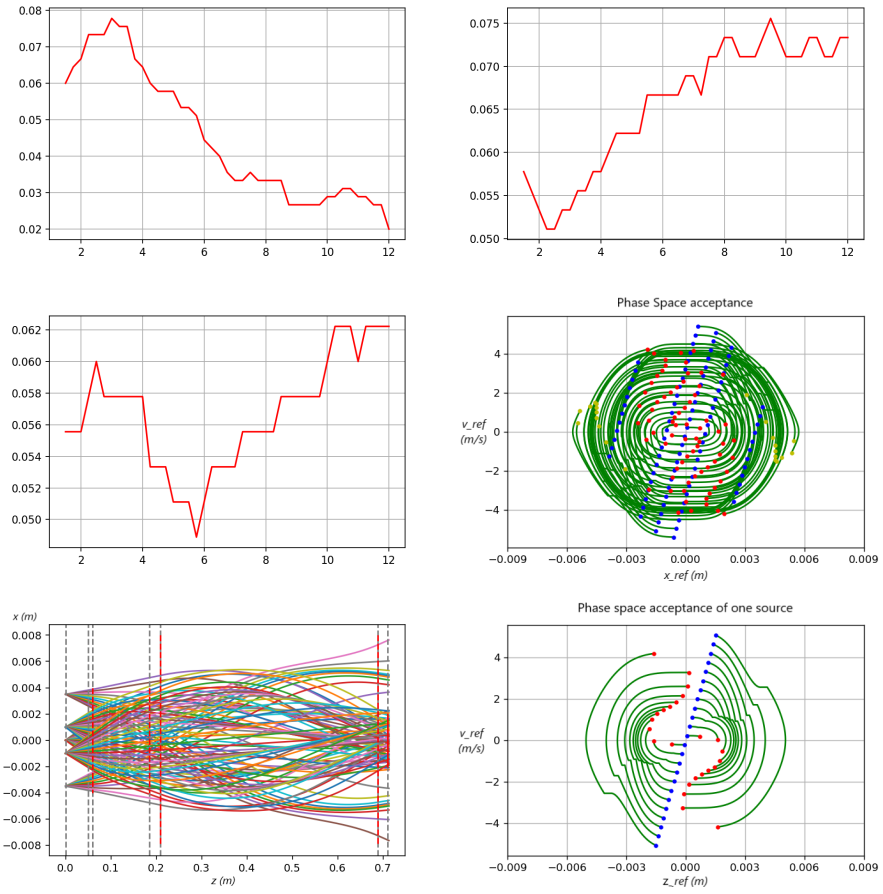

Figure 33: Per applied voltage 900 particles are generated for these graphs. Top Left : Decelerators acceptance of the guided molecules for different applied voltages to the front guide (kV) with inner radius of 4 mm. Max acceptance: 7.78% at applied voltages of 3 kV. Top Right: Decelerators acceptance of the guided molecules for different applied voltages to the front guide (kV) with inner radius of 8 mm. Max acceptance: 6.22% at applied voltages of 10.25∼12 kV. Middle Left: Decelerators acceptance of the guided molecules for different applied voltages to the front guide (kV) with inner radius of 6 mm. Max acceptance: 7.56% at applied voltages of 9.5 kV. Middle Right: we see the phase space transformation of the 7.78% of the 4 mm case. Bottom Left: The trajectory of the molecules that make it into the guide for the 4 mm. Bottom Right: We see the phase space transformation of the 7.78% of the 4 mm case. But this time with only one source to see the phase space transformation clearly.

Now there is only one thing left to do, namely exploring the rear hexapole again with this 4 mm front hexapole at 3 kV. This is done in Fig. 34.

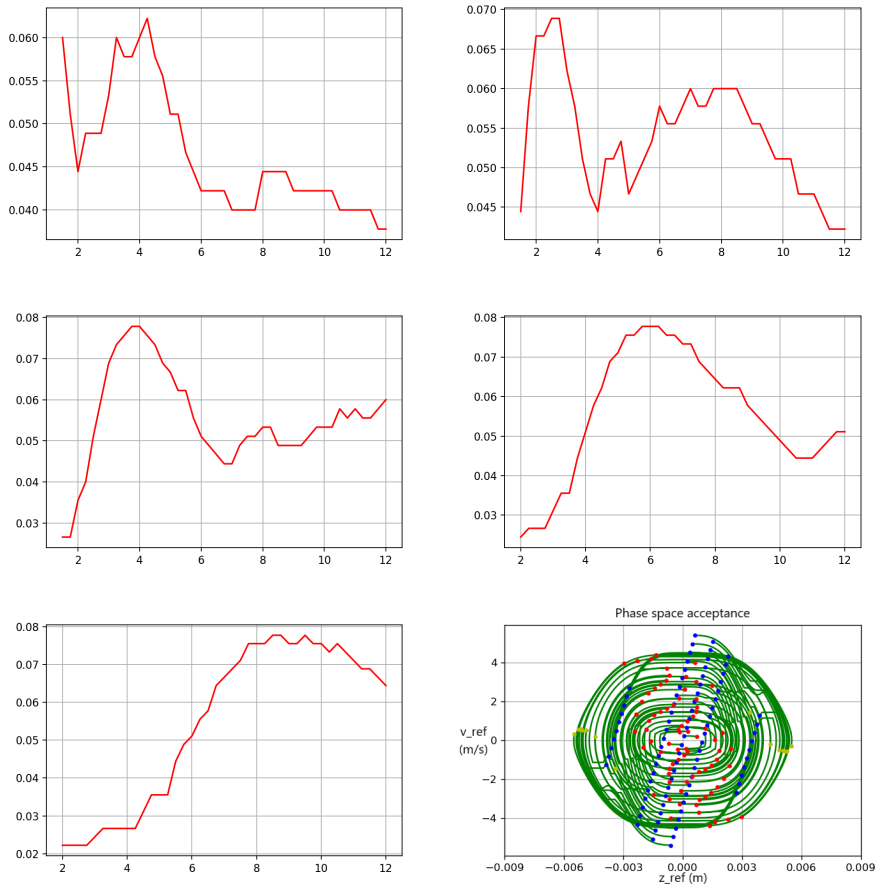

Figure 34: Per applied voltage 900 particles are generated for these graphs. Top Left: Decelerators acceptance of the guided molecules for different applied voltages to the rear guide (kV) with inner radius of 4 mm. Max acceptance: 6.22% at applied voltages of 4.25 kV. Top Right: Decelerators acceptance of the guided molecules for different applied voltages to the rear guide (kV) with inner radius of 5 mm. Max acceptance: 6.89% at applied voltages of 2.5-2.75 kV. Middle Left: Decelerators acceptance of the guided molecules for different applied voltages to the rear guide (kV) with inner radius of 6 mm. Max acceptance: 7.78% at applied voltages of 3.75-4 kV. Middle Right: Decelerators acceptance of the guided molecules for different applied voltages to the rear guide (kV) with inner radius of 7 mm. Max acceptance: 7.78% at applied voltages of 5.75-6.25 kV. Bottom Left: Decelerators acceptance of the guided molecules for different applied voltages to the rear guide (kV) with inner radius of 8 mm. Max acceptance: 7.78% at applied voltages of 8.5-8.75, 9.5 kV. Bottom Right: we see the phase space transformation of the 7.78% of the 6 mm case. This should be almost the same phase space as in Figure 33.

6 Gauss Distribution

Let us try to also upgrade the source generation. Until now a fan function was used to represent reality. Now a more realistic Gauss distribution is used with a longitudinal velocity of about $v_l = 200 \pm 50\ m/s$, so with a FWHM spread of about 100 m/s, and transversal (v_t) as stated above. With the previous gotten results we got a good range of where we need to search to get the highest acceptance. For the Gauss distribution and when there is no guide activated in the deceleration experiment: The acceptance of the decelerator of 10000 molecules coming out of the source is 3.7% (370 molecules). Therefore, the loss factor is 27.

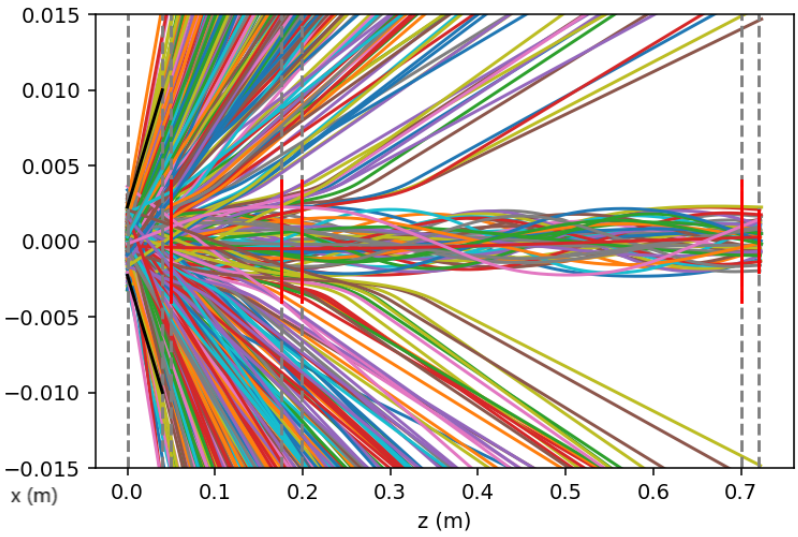

Figure 35: *The Gauss distribution shows how well it works for guiding.*

6.1 Long Front Guide

From the NL-eEDM there was an interest in investigating a long front guide of 50 cm case for the simulations. Therefore, an additional range of simulations is done for this for both the hexapole and the quadrupole case. For this simulation, a pipe needs to be added to the experimental setup. Now from the entrance of the guide there is a 50 cm long guide with 2 mm of room for the valve (24 mm wide) and then 80 mm to the decelerators entrance. The phase space acceptance is measure 3 mm inside the decelerator, because this is roughly the region where the minimal of the separatrix is at. For both Figure 36 & 37, the vertical and horizontal axis have the same function as the graphs depicted before.

From section 6.1.1 & 6.1.2 we can only make broad assumptions. The error between the values and the crashes render these results to be unreliable. This will be further discussed in section 8.

6.1.1 Quadrupole 50cm Long Front Guide

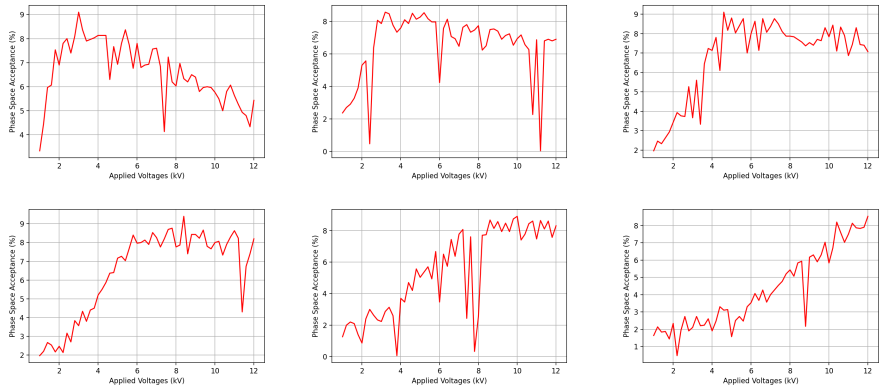

Figure 36: Decelerators acceptance of the guided molecules for different applied voltages (kV) at different radii at the vertical axis. 5000 molecules are generated per applied voltage. With steps of 0.1 kV. Please note that the extreme peaks down are where the code crashes. So, these values are discarded.

6.1.2 Hexapole 50cm Long Front Guide

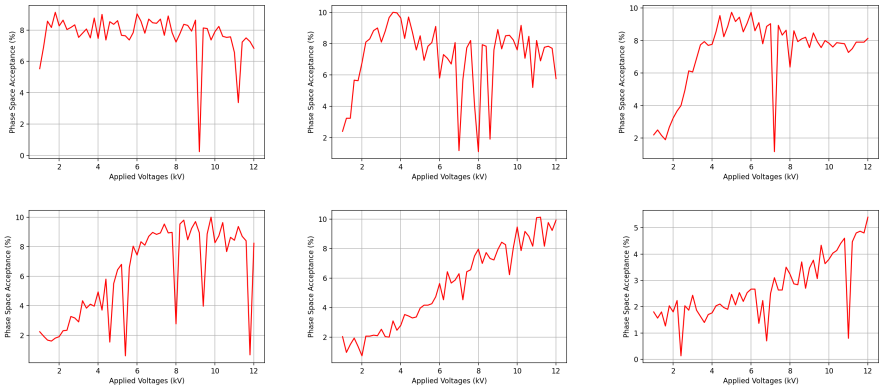

Figure 37: Decelerators acceptance of the guided molecules for different applied voltages (kV) at different radii at the vertical axis. 5000 molecules are generated per applied voltage. With steps of 0.1 kV. Please note that the extreme peaks down are where the code crashes. So, these values are discarded.

6.2 Combining Front and Rear Guide Results

From section 4.5.1 we know that a front hexapole guide of 4 mm inner radius at ± 6,5 kV gives the highest acceptance. With this front guide we will test different hexapole rear guides and see which one will give the highest acceptance. Because these simulations are probably going to give the highest acceptance. From the Gauss distribution it looks like the 4 mm inner radius for both the front and rear guide is the most efficient. The graphs give the values of the acceptance of the decelerator of the rear guide variation of the radii from 4 mm to 10 mm. And it is visible that both the 4 mm and 5 mm inner radius gave the highest acceptance.

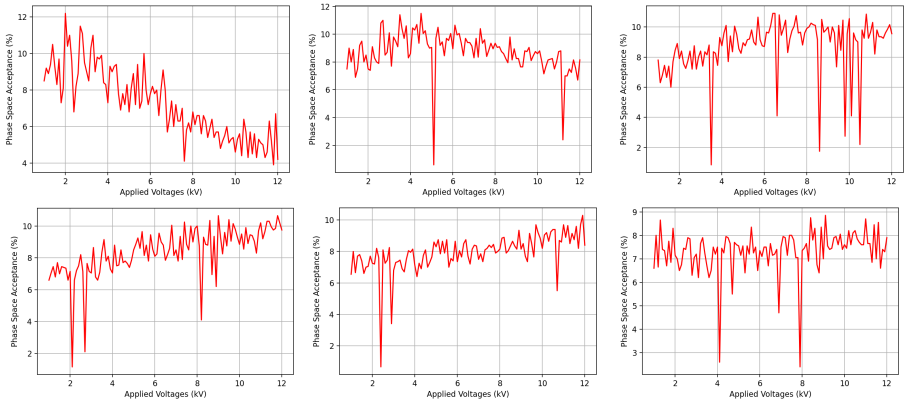

Figure 38: Decelerators acceptance of the guided molecules for different applied voltages (kV) at different radii at the vertical axis. 5000 molecules are generated per applied voltage. With steps of 0.1 kV. Please note that the extreme peaks down are where the code crashes. So, their values are discarded.

7 Future Goals

Obviously many future research options are still left. The $|N, m_N\rangle = |20\rangle$ state was still planned to be researched thoroughly. The data was acquired by the author in the last week of the research. Therefore, time shortages made this impossible, nonetheless. The code is already written and put on a git server for the team to be used if this is desired.

Also, the Gauss distribution was still in the planning to be researched thoroughly. Now the code finally works it can be used to make too make more simulations realistic with noisy data. Therefore, future simulations can be done. But because they have given the same overall results, it is not expected that these simulations will given another conclusion.

Many Geometries are not researched yet but are interesting. It might be smart to look at a 25 cm front guide and 25 cm rear guide situations. Although making the front guide longer has not proven to increase the acceptance in previous research, maybe in this configuration the molecules loss is much smaller.

8 Discussion

The consequences that the different property and simulation choices have on the final result will be taken in consideration here by looking at the limitations of the guide, the interpretations of the results, the overall understanding of the received results and the given constrains by the experiment. What happens in detail to the guide is stated in the results section.

8.1 Electric Field Edge Effects

We have some error in our electric field formula, because of the use of our equations for the electric field are simpler than in reality the electric field actually is. This must be done, otherwise the computer will take hours or days to compute the results. The negative side effect is that the beginning and ends of the guide have the same electric field distribution as in the middle. This is obviously not as it is in reality. The same goes for the region of free-flight, in this region there is truly free-flight. Therefore, there is no electric field effects from the guide in region. So, in the simulations we ignore the so-called edge effects of the diminishing electric field at the edges of the guide.

When we look at the effects of this true free flight in the phase space diagrams. It is concluded that the effect of both these edge effects have minimal effect on the molecule's trajectory. This is probably mainly due to the heavy nature of the BaF molecules and the noticeably short distances this is a problem. Because the molecule is so heavy, it needs a lot of force to be guide correctly, if there are small regions where the electric field is larger or smaller than it in reality should be. We conclude that if these effects would have had any effects on the molecule's trajectory, then these effects will cancel each other out to such

a small margin that we can easily neglect these errors in the simulation. But for future simulations these effects can be added to the simulation if that is desired.

8.2 Source Creation

8.2.1 Simple Code

Reading through the thesis, it is probably noticed that there is much written about the source from which the molecules come. Like in section 3 a simple fan like source was created. As the reasons why this was done are stated in this section, lets talk about the assumptions and errors. This fan like distribution has limitations in its distribution as well as positive side effects. The locations and velocities in this distribution are not random like in the Gauss distribution, but they are always the same when the same variables are put in. Thus, making the results easier reproducible for checking certain values and theories.

The obvious drawback therefore is that our actual source will never be anything like this source, because the fan is totally dependent on the start position and given velocities of the molecules. And therefore, the acceptance can be viewed as the function of the start positions and velocities in the fan like distribution. This is not how the source works in reality. The plus side of this is that the analysis of the phase space transformation is clear. And that these properties work very well with Liouville's theorem.

Saying that this distribution will never be anything like our actual source may sound bad, but it depends on how you look at it. The distribution will have the right distribution of transversal and longitudinal velocities that make it through the guide and are successfully decelerated. And when we switch from different source generation this does not change. Therefore, this makes a great steppingstone for our Gauss and we do not have to do for every possible variable a reexamination of the gotten acceptance.

8.2.2 Slow code

A drawback is that this fan was made with transversal velocities that would never have reached the outside of the source. This is due to that some circumstances were not revealed till late in the projects research. This inconvenience has no serious effects on the end result, nonetheless. As this ranges from 25 m/s too 50 m/s and then especially the higher ranges within that, these molecules would never be guided properly in the decelerator, as these velocities are much too high and molecules will just end up colliding with the electrodes of the decelerator.

Last point; because the code needed to do many derivations per simulation, the overall molecules created in every simulation are not as high as in the advanced code. Even with this diminished amount of molecules, the simulations sometimes took up to six hours to compute.

8.2.3 Advanced Code

Most of the points raised in the section above have been bypassed or solved with our more advanced code. The last comment about this Gauss distribution is that it is still not the actual data points gotten from the source. Therefore, there is still an error within the acceptance of the decelerator when it would be compared to reality.

This could be solved with further examination. Unfortunately, this is outside the scope of this thesis. But the code is written in such a way that it is not difficult to be put into the code. This could be done with some minor adjustments to the code and then a data file can be analysed. Therefore opening the way to even more accurate simulations of the guide.

A well-known problem when you make a code more complex is that, simulations have a higher chance of having bugs in them. This sometimes happened for this code. The problem leading to this has sadly not been found. If there are bugs in a calculation, it will be noted underneath the graphs. These bugs are very distinctively present in the acceptance graphs. When the simulation breaks down it will only be done with checking a part of all the molecules. Therefore, the extremely low peaks shooting down are almost always a bug, but not every single time. The bug is noted in python by an error about the dimensions of an array and its size. The amount of times this happened could be seriously lowered by altering some begin values but not all the bugs were gone after doing that. The bugs make the results unreliable but not wrong. Still the Max. and Min. are distinguishable and do agree with the results found by the fan distribution. Therefore, it will be considered in the conclusion. Not for its precise value but for its overall checking of the correctness of the data. It is advised to the person that wants to work further with these simulations to try and solve the problem themselves.

Day of the hand in of this thesis the solution was found, for this beautiful Gauss distribution look at Figure 35. Sadly, more time was left to complete any simulations. The problem was that the initial conditions of a Gauss distribution could not be handled as a regular function. The author's prior knowledge of Python before he began this project was zero. Hence that it took this long to construct this entire code and took much longer to find and fix the bugs.

8.3 Chosen Geometries

In the thesis it can be noticed that the simulations are done for an extremely specific range of inner radii, guide lengths, rod radii and number of rods. This is due to that the NL-eEDM team is allowed to use some pre-existing building guides. And therefore, their geometries have the preference to be tested. The best and most efficient guide may not be in the range where now is searched in. This is unfortunate, but in order to search the whole range of the geometries it would simply take too much time. For future experimentation, these ranges can be further explored and a higher acceptance may be found in this range.

8.4 Tools Worked With

The simulations are not finished as far as the author would have liked. But even though the circumstances were not always ideal the author still managed to get far. Due to the corona virus no personal meeting with the NL-eEDM team was possible. All was done online, making a difficult task even more challenging.

This was particularly noticeable in the communication between the team. All the constraints and boundary conditions had to be acquired from colleagues and checked. At some point the whole project was written and done, but then newly acquired information about the given function of the electric field meant all had to be redone. Also, this same situation occurred with the discovery of the first hole in the cryogenic source. These consumed weeks of work done, each time. The advice is to give the bachelor student, whom does this practical project more information about the set-up of the whole system, before the student embarks on a search to the answers. From this the author learned much and now knows very specific details of the project. But with this it also meant that the project is not as finished as the author would have liked.

The strong advice this thesis will give is that, personal contact in real life is paramount for good research. Therefore, the advice to the NL-eEDM team is to get together every day again and discuss what you are doing. Obviously within the restrictions of the 1.5 m rules.

All the results are saved for further research. If any results are desired, then the author can be contacted for this.

9 Conclusion

From the simulations done it can be concluded that for a short front guide the hexapole of 4 mm inner radius must be chosen. At the applied voltage of 6.5 kV it gave the highest acceptance. Also, for an extended front guide, the hexapole (of radii 6-8 mm) gave the highest acceptance.

From the rear guide simulations, it was concluded that short rear guides had such a low impact that they were removed from the thesis. This left the experiment with the long rear guide. Again, the hexapole gave the highest acceptance. This time at an inner radius of 7 mm at the applied voltage of 5.6 kV.

When different combinations of front and rear guides were tested, always the hexapole and hexapole guide gave the highest acceptance. Therefore, with all these given conclusions, it can be safely assumed that this will always be the case in this situation for the molecule Barium Mono-Fluoride.

After combining the results in section 4.6, the best configuration is concluded for our simulation. With the 4 mm hexapole in the front at applied voltage of 6.5 kV. The highest overall acceptance was measured at 11.4% for the 50 cm rear radii of 4-7 mm. With the 4 mm rear inner radius there is even a 99.1% found, for the guided molecules that reach the decelerators acceptance. This is therefore a decrease of the overall loss factor from 29 to 8.8. Thus, the loss can be decreased with a factor of 3.3 with this configuration. This is also the highest possible increase in particles one could get with adding a guide. This increased factor of molecules is considered significant enough to have the guide being placed in the set-up as it is now.

Therefore, the advice to the NL-eEDM team is to place two guides. The front guide has to be a 125 mm hexapole of 4 mm inner radius at applied voltage of 6.5 kV. And the rear guide has to be a 50 cm hexapole of 4 mm inner radius at applied voltage of 6.9 kV. In Figure 29 this situation is displayed.

10 Acknowledgements

The results reported in this paper would not have been possible without the outstanding performance of the NL-eEDM team, the Rijksuniversiteit of Groningen, and the Van Swinderen Institute. A big thanks is also needed for the following colleagues from the Vrije Universiteit Amsterdam: Prof. Dr. H.L. Bethlem and Wander van der Meer. And for the following colleague bachelor student of the Rijksuniversiteit of Groningen: Bart Schellenberg.

References

[1] H. Rechenberg, *The Historical Development of Quantum Theory*, ser. The Historical Development of Quantum Theory. Springer, 2001, no. v. 1-2. [Online]. Available: https://books.google.nl/books?id=8tUVMSsC9wAC

[2] B. Friedrich and D. Herschbach, "Stern and gerlach: How a bad cigar helped reorient atomic physics," *Physics Today, 53-59 (2003)*, vol. 56, p. 6, 12 2003. [Online]. Available: http://www.fhi-berlin.mpg.de/mp/friedrich/PDFs/ptsg.pdf?fbclid=IwAR3G1pjcmql_inPrkA-QMkQK_0SfNOljzvMJK03WqDP_ecOPwWndlYS4Wb8

[3] O. Stern and W. Gerlach, "Der experimentelle nachweis der richtungsquantelung im magnetfeld," *Zeitschrift für Physik*, vol. 9, pp. 349–352, Dec 1992. [Online]. Available: https://doi.org/10.1007/BF01326983

[4] "Observation of a new particle in the search for the standard model higgs boson with the atlas detector at the lhc," *Physics Letters B*, vol. 716, no. 1, pp. 1 – 29, 2012. [Online]. Available: http://www.sciencedirect.com/science/article/pii/S037026931200857X

[5] K. Abe, R. Akutsu, A. Ali, and et al, "Constraint on the matter–antimatter symmetry-violating phase in neutrino oscillations," *Nature*, vol. 580, no. 5, pp. 339–344, 2020. [Online]. Available: https://doi.org/10.1038/s41586-020-2177-0

[6] M. Pospelov and A. Ritz, "Electric dipole moments as probes of new physics," *Annals of Physics*, vol. 318, no. 1, pp. 119 – 169, 2005, special Issue. [Online]. Available: http://www.sciencedirect.com/science/article/pii/S0003491605000539

[7] P. Aggarwal, H. Bethlem, A. Borschevsky, M. Denis, K. Esajas, P. Haase, Y. Hao, S. Hoekstra, K. Jungmann, T. Meijknecht, M. Mooij, R. Timmermans, W. Ubachs, L. Willmann, and A. Zapara, "Measuring the electric dipole moment of the electron in baf," *The European Physical Journal D*, vol. 72, 2018. [Online]. Available: https://doi.org/10.1140/epjd/e2018-90192-9

[8] N. R. Hutzler, M. F. Parsons, Y. V. Gurevich, P. W. Hess, E. Petrik, B. Spaun, A. C. Vutha, D. DeMille, G. Gabrielse, and J. M. Doyle, "A cryogenic beam of refractory, chemically reactive molecules with expansion cooling," *Phys. Chem. Chem. Phys.*, vol. 13, pp. 18 976–18 985, 2011. [Online]. Available: http://dx.doi.org/10.1039/C1CP20901A

[9] N. E. Bulleid, S. M. Skoff, R. J. Hendricks, B. E. Sauer, E. A. Hinds, and M. R. Tarbutt, "Characterization of a cryogenic beam source for atoms and molecules," *Phys. Chem. Chem. Phys.*, vol. 15, pp. 12 299–12 307, 2013. [Online]. Available: http://dx.doi.org/10.1039/C3CP51553B

[10] L. D. van Buuren, C. Sommer, M. Motsch, S. Pohle, M. Schenk, J. Bayerl, P. W. H. Pinkse, and G. Rempe, "Electrostatic extraction of cold molecules from a cryogenic reservoir," *Phys. Rev. Lett.*, vol. 102, p. 033001, Jan 2009. [Online]. Available: https://link.aps.org/doi/10.1103/PhysRevLett.102.033001

[11] S. van de Meerakker, H. Bethlem, N. Vanhaecke, and G. Meijer, "Manipulation and control of molecular beams," *Chemical Reviews*, vol. 112, no. 9, pp. 4828–4878, 2012, van de Meerakker, Sebastiaan Y. T. Bethlem, Hendrick L. Vanhaecke, Nicolas Meijer, Gerard.

[12] D. J. Griffiths, *Introduction to electrodynamics; 4th ed.* Boston, MA: Pearson, 2013, re-published by Cambridge University Press in 2017. [Online]. Available: https://cds.cern.ch/record/1492149

[13] J. Kalnins, G. Lambertson, and H. Gould, "Improved alternating gradient transport and focusing of neutral molecules," *Review of Scientific Instruments*, vol. 73, no. 7, pp. 2557–2565, 2002. [Online]. Available: https://doi.org/10.1063/1.1485778

[14] R. W. Anderson, "Tracks of symmetric top molecules in hexapole electric fields," *The Journal of Physical Chemistry A*, vol. 101, no. 41, pp. 7664–7673, 1997. [Online]. Available: https://doi.org/10.1021/jp971313s

[15] J. M. Brown and A. Carrington, *Rotational Spectroscopy of Diatomic Molecules.*, ser. Cambridge Molecular Science Series. Cambridge University Press, 2003. [Online]. Available: http://search.ebscohost.com.proxy-ub.rug.nl/login.aspx?direct=true&db=nlebk&AN=120308&site=ehost-live&scope=site

[16] C. Effantin, A. Bernard, J. d'Incan, G. Wannous, J. Vergès, and R. Barrow, "Studies of the electronic states of the baf molecule," *Molecular Physics*, vol. 70, no. 5, pp. 735–745, 1990. [Online]. Available: https://doi.org/10.1080/00268979000101311

[17] C. Ryzlewicz and T. Törring, "Formation and microwave spectrum of the 2-radical barium-monofluoride," *Chemical Physics*, vol. 51, no. 3, pp. 329 – 334, 1980. [Online]. Available: http://www.sciencedirect.com/science/article/pii/0301010480801078

[18] W. E. Ernst, J. Kändler, and T. Törring, "Hyperfine structure and electric dipole moment of baf $x^2\sigma^+$," *The Journal of Chemical Physics*, vol. 84, no. 9, pp. 4769–4773, 1986. [Online]. Available: https://doi.org/10.1063/1.449961

[19] J. Maat, *Calculations on the energy level structure and the effects of external fields in barium monofluoride and The design and construction of an optical trap for nanoparticles as vibration sensors.* University of Groningen, 2018. [Online]. Available: http://fse.studenttheses.ub.rug.nl/17738/

[20] B. Schellenberg, *An Analytic Analysis of a Traveling-wave Stark Decelerator*. University of Groningen, 2020.

[21] J. Liouville, "Note sur la théorie de la variation des constantes arbitraires." *Journal de Mathématiques Pures et Appliquées*, pp. 342–349, 1838. [Online]. Available: http://eudml.org/doc/234417

[22] F. M. Crompvoets, H. L. Bethlem, and G. Meijer, "A storage ring for neutral molecules," ser. Advances In Atomic, Molecular, and Optical Physics, P. Berman and C. Lin, Eds. Academic Press, 2005, vol. 52, pp. 209 – 287. [Online]. Available: http://www.sciencedirect.com/science/article/pii/S1049250X05520056

[23] W. Ketterle and D. E. Pritchard, "Atom cooling by time-dependent potentials," *Phys. Rev. A*, vol. 46, pp. 4051–4054, Oct 1992. [Online]. Available: https://link.aps.org/doi/10.1103/PhysRevA.46.4051

[24] P. K. Kundu, I. M. Cohen, and D. R. Dowling, *Fluid Mechanics sixth Ed.* Academic Press, 2016.

[25] Private communications with Prof. Dr. H.L. Bethlem, 2020.

[26] Private communications with Y.Yin, 2020.

[27] Private communications with L. Huisman, 2020.